Cessation of Southern Ocean deep convection under anthropogenic climate change

Casimir de Lavergne

Masters of Science

Atmospheric and Oceanic Sciences

McGill University

Montreal, Quebec

2012-05-30

A thesis submitted to the Faculty of Graduate Studies and Research in partial fulfillment of the requirements for the degree of Master of Science

ACKNOWLEDGEMENTS

This work was supported by the Stephen and Anastasia Mysak Graduate Fellowship in Atmospheric and Oceanic Sciences and by the department of Atmospheric and Oceanic Sciences. I would like to thank Professor Lawrence Mysak for his generosity, which enabled me to carry out my masters under privileged conditions. I am also grateful to my supervisors, Jaime Palter and Eric Galbraith, for providing me the opportunity to work on this important project and for their patient guidance and advice throughout its realization. This project would not have been possible without the active collaboration of Raffaelle Bernardello and Irina Marinov. I also thank Simon Yang for his help with model runs and Daniele Bianchi for his availability and precious help with the analysis.

CONTRIBUTION OF AUTHORS

This thesis is based on a co-authored manuscript: C. de Lavergne, J. B. Palter, E. D. Galbraith, R. Bernardello and I. Marinov, Cessation of Southern Ocean deep convection under anthropogenic climate change, submitted to *Nature Geoscience*. Specifically, the present work incorporates the main body and supplementary material of the above-mentioned manuscript, while expanding on a number of aspects. The introductory chapter, Figure 3.3 and its discussion, the second and fourth paragraphs of the last chapter and Appendix B include the most important additions. C. de Lavergne retrieved CMIP5 data, completed the analysis of all CMIP5 and CM2Mc model simulations, shared responsibility for writing the original manuscript and owns responsibility for all modifications and additions included in the present thesis. Eric Galbraith and Jaime Palter conceived the study and shared responsibility for writing the original manuscript. R. Bernardello performed the CM2Mc climate change experiments and shared responsibility for writing the original manuscript. I. Marinov shared responsibility for writing the original manuscript.

ABSTRACT

In 1974, newly available satellite observations unveiled the presence of a giant ice-free area within the Antarctic ice pack, which persisted throughout the winter, and formed again in the next two winters. Subsequent research showed that deep convective overturning kept the waters ice-free, through the massive release of heat rising from the deep sea. While the polynya has aroused continued interest among climate scientists, it has not reappeared since 1976. Here we use model experiments to show that deep convection in the Southern Ocean, common in current generation climate models, is highly sensitive to anthropogenic forcing, and ceases in many models when forced by a high emissions climate change scenario. The slowdown in deep ventilation follows from the gradual freshening of polar surface waters, a trend which is borne out by observations over recent decades. Our results suggest that deep convection in the Southern Ocean will be less common in future, and may have already been significantly reduced compared to the pre-industrial period, with important consequences for ocean circulation and climate.

RÉSUMÉ

En 1974, des observations satellite nouvellement disponibles révélèrent la présence d'une géante surface d'eau libre au sein de la glace de mer entourant l'Antarctique, qui persista tout au long de l'hiver et réapparut les deux hivers suivants. Les recherches qui suivirent montrèrent que les eaux étaient maintenues libres de glace par la convection profonde, permettant à une grande quantité de chaleur de remonter des profondeurs pour être ensuite libérée dans l'atmosphère. Si la polynya continue de susciter l'intérêt des climatologues, elle n'est cependant pas réapparue depuis 1976. Nous utilisons ici des expériences de modélisation pour montrer que la convection profonde dans l'Océan Austral, commune dans les modèles de climat actuels, est fortement sensible au forçage anthropique, et cesse dans beaucoup de modèles quand ceux-ci sont forcés par un scénario de fortes émissions. Le ralentissement de la ventilation profonde résulte de la baisse progressive de la salinité des eaux de surface, une tendance corroborée par les observations des dernières décennies. Nos résultats suggèrent que la convection profonde dans l'Océan Austral sera moins fréquente dans le futur, et a peut-être déjà été significativement affaiblie relativement à la période préindustrielle, avec d'importantes conséquences pour la circulation océanique et le climat.

TABLE OF CONTENTS

LIST OF TABLES

LIST OF FIGURES

(5-year mean following convection minus 5-year mean preceding convection). The pink line encircles the convection area (600 m annual mixed layer contour). **D**, Ocean temperature anomaly (°C) at 40°W associated with deep convection, with respect to the non-convective state. Deep convective state corresponds to years with a maximum 73°S-68°S; 50°W-30°W annual mixed layer depth greater than 1400 m, whereas non-convective state refers to years with an average 73°S-68°S; 50°W-30°W annual mixed layer depth less than 200 m. Note the strong Southern Hemisphere warming associated with convection and apparent teleconnections with Northern Eurasia (**A**). The dipole of ocean temperature anomalies in **D** is due both to convective heat release and southward shift of the Antarctic Circumpolar Current (ACC) compensating for the deep outflow from the Weddell Sea. Note that this cooling/warming dipole results in an increase of the local meridional density gradient and thereby of the ACC transport. Additionally, the warming of the high latitude atmosphere during convection (**A**, **B**) reduces the meridional temperature gradient, weakening the storm tracks [Yin, 2005] and the low-level atmospheric circulation [Latif *et al.*, in press]. (Conversely, note that a convection halt would contribute to a positive trend in the Southern Annular Mode - a potential positive feedback to the surface freshening responsible for convection cessation in climate change simulations.) 48

Figure B.3: Evolution of Weddell Sea (73°S-68°S; 50°W-30°W average) annual mixed layer depth (black) and AABW transport at 20°S in the Atlantic (red) over 500 years of a CM2Mc pre-industrial control simulation. AABW transport is calculated as the minimum of the Atlantic meridional overturning streamfunction at 20°S and smoothed with a 10-year running mean. Pulses of Antarctic Bottom Water transport are seen to follow each convection event. The maximum correlation is 0.7486 with a lag of +27 years: it takes about 30 years for most of the deep water formed in the Weddell Sea to be exported to 20°S in the South Atlantic. 49

Figure B.4: Evolution of Weddell Sea (73°S-68°S; 50°W-30°W average) annual mixed layer depth (black) and NADW transport at 20°S (blue) over 500 years of a CM2Mc pre-industrial control simulation. NADW transport is calculated as the maximum of the Atlantic meridional overturning streamfunction at 20°S and smoothed with a 10-year running mean. The max correlation is -0.7418, with a lag of + 14 years: a low in NADW transport at 20°S follows a convective event by 14 years. Both upper and lower limbs of the Atlantic meridional overturning respond to Weddell Sea convective events, resulting in a seesaw in AABW and NADW transport (with the minimum in NADW transport leading the maximum in AABW transport by ~13 years). Following convection a large inflow of AABW raises isopycnals in the South Atlantic, increasing the slope of

Chapter 1

Introduction

Deep water formation occurs in essentially two different ways [Killworth, 1983]. The first process takes place on continental margins, and involves the salt-enrichment of shelf waters during sea-ice formation and their subsequent mixing with ambient waters while exported in downslope currents. The second pathway consists in deep winter convection in the open ocean, when surface heat loss reduces the buoyancy of surface waters sufficiently to let them sink in convective plumes, gradually mixing and cooling the whole water column. In the North Atlantic, both pathways contribute to the ventilation of North Atlantic Deep Water (NADW) [Kuhlbrodt *et al.*, 2007]. Deep convection occurs primarily in the Labrador Sea, and occasionally in the Greenland Sea [Marshall and Schott, 1999]; the remaining contribution to NADW is provided by dense waters overflowing from the Nordic Seas [Meincke *et al.*, 1997]. In contrast, the denser deep waters of Southern Hemisphere origin, collectively referred to as Antarctic Bottom Water (AABW), are presently solely produced on Antarctic continental shelves [Orsi *et al.*, 1999]. Four distinct sites have been identified: the western Weddell Sea, the Ross Sea, Adélie Coast and Cape Darnley.

In 1928, Wüst [Wüst, 1928] cast doubt on the ability of shelf-processes to produce all of the observed AABW, hypothesizing that open ocean convection should also contribute to its formation, as occurs in the Northern Hemisphere. He argued that convection must occur within the Weddell gyre, where the background circulation and stratification are favourable to the onset of convective instabilities [Killworth, 1979]. Observational support for his hypothesis did not come until the mid-1970s, when early microwave satellite observations revealed the opening of a 250,000 km^2 ice-free area within the seasonally ice-covered Weddell Sea [Carsey,

1980]. The huge polynya, located near Maud Rise (65°S, 0°E), reappeared in the same region for three consecutive winters, showing that it was a relatively stationary feature of the ocean over that time, rather than a result of wind forcing [Carsey, 1980]. The polynya was maintained by vigorous convective mixing, whereby the upward flux of relatively warm deep waters supplied enough heat to prevent sea ice formation [Gordon, 1978]. Heat loss at the surface drove cooling to depths of about 3000 m, producing deep waters at an estimated rate of 1.6-3.2 Sverdrups (Sv) over the three-year period [Gordon, 1982]. These observations appeared to confirm that deep convection in the open Weddell Sea was an important mode of AABW ventilation [Killworth, 1983; Martinson, 1991]. However, following 1976, the polynya was not observed again, despite continuous satellite monitoring. Weddell Sea convection is now generally assumed to be an uncommon phenomenon [Marshall and Schott, 1999], perhaps to return when the leading modes of climate variability again converge to the appropriate conditions [Gordon *et al.*, 2007].

Measurements of chlorofluorocarbon concentrations from the past three decades have provided means to assess the present global rate of AABW and NADW production, which lie broadly within 5-10 Sv and 15-20 Sv, respectively [Orsi *et al.*, 1999; Orsi *et al.*, 2002; Smethie and Fine, 2001; LeBel *et al.*, 2008]. The larger volume [Johnson, 2008] but slower formation rate of AABW relative to NADW suggests however that AABW production must have been stronger in the past. Indeed, there is strong evidence of a widespread warming and concomitant volume contraction of AABW over the past three decades [Purkey and Johnson, 2012]. The inferred rate of AABW volume contraction of 8 ± 2.6 Sv, comparable to the present global formation rate, indicates that most of the decrease in AABW ventilation must have occurred prior to the 1980s [Purkey and Johnson, 2012]. This is consistent with the apparent steadiness of bottom water production from the Antarctic shelves over the observational period [Gordon *et al.*, 2001; Whitworth and Orsi, 2006; Williams *et al.*,

2008, Ohshima *et al.*, 2013; Huhn *et al.*, 2013]. Yet, given the probable halving of AABW formation during the 20th century, it is puzzling that shelf-production has shown relatively little sensitivity to recent climate change. The resolution to this puzzle could lie in the loss of open ocean convection as an important mode of Southern Ocean deep ventilation, a possibility that has received little attention to date, and the hypothesis we present here.

Chapter 2 describes the methodology used and the characteristics of Southern Ocean deep convection in state-of-the-art climate models. In Chapter 3, we explore the response of the deep convection to anthropogenic climate change. Implications and conclusions are presented in Chapter 4.

Chapter 2

Open ocean convection in model simulations

Recurring convective events in the circum-Antarctic have been remarked upon in some coupled ocean-atmosphere models, particularly in the Weddell Sea [Galbraith *et al.*, 2011; Martin *et al.*, 2012]. In order to ascertain whether these convective events are common among the current generation of climate models, we examined 36 models of the most recent Coupled Model Intercomparison Project (CMIP5) [Taylor *et al.*, 2012].

2.1 Methods

We analyzed all CMIP5 models where 'historical' and 'rcp85' experiments with potential temperature, salinity and sea ice concentration monthly fields were available. Model outputs were downloaded from the Program for Climate Model Diagnosis and Intercomparison data portal at http://pcmdi9.llnl.gov/esgf-web-fe/ [Taylor *et al.*, 2012]. Only one run per model and per experiment ('r1i1p1') was considered. Since ensembles were not available for all models and all experiments, this enabled to treat all models homogenously, while the large number of models considered was deemed to provide a sufficient overall ensemble of climate change simulations. Historical (1860-2005) and RCP8.5 (2006-2100) outputs were concatenated to obtain 1860-2100 time series. Eight models had extended RCP8.5 integrations (2006-2300). A listing of all the models used is shown in Table 2.1.

Historical experiments include the full range of natural and anthropogenic forcings, consistent with observations. RCP8.5, or Representative Concentration Pathway 8.5, corresponds to a high emissions scenario that includes time-varying greenhouse gas, ozone, aerosol, and solar forcings [Meinshausen *et al.*, 2011]. Under RCP8.5, the radiative forcing relative to pre-industrial conditions rises continuously

Models	Maximum convection area (10^5 km^2)	Mean convection area (10^5 km^2)	Atlantic sector fraction (%)	Indian sector fraction (%)	Western Pacific sector fraction (%)	Eastern Pacific sector fraction (%)
ACCESS1.0	14.20	7.98	84.3	1.6	14.1	0.0
ACCESS1.3	18.48	9.05	68.8	1.9	29.6	0.0
BCC-CSM1.1	18.88	4.08	83.4	16.0	0.0	0.0
BCC-CSM1.1m	32.68	11.18	81.7	18.3	0.0	0.0
CMCC-CM	14.05	4.55	88.5	11.4	0.0	0.0
CMCC-CMS	12.75	1.50	58.3	41.7	0.0	0.0
CNRM-CM5	13.48	1.00	100.0	0.0	0.0	0.0
FGOALS-g2	3.80	0.45	0.0	5.6	94.4	0.0
FGOALS-s2	46.95	35.85	84.9	13.6	0.6	0.0
GFDL-CM3	25.00	8.15	28.5	0.9	69.6	0.6
GFDL-ESM2G	27.55	12.43	59.6	40.4	0.0	0.0
GFDL-ESM2M	17.55	8.78	85.8	14.2	0.0	0.0
GISS-E2-H	18.65	10.43	14.6	42.9	42.2	0.0
GISS-E2-R	58.60	47.85	28.9	24.5	40.3	6.3
HadGEM2-AO	5.73	0.40	100.0	0.0	0.0	0.0
HadGEM2-CC	4.33	0.70	92.9	0.0	3.6	0.0
HadGEM2-ES	3.55	0.45	88.9	0.0	16.7	0.0
IPSL-CM5A-LR	10.53	0.75	3.3	10.0	16.7	70.0
IPSL-CM5A-MR	14.68	2.53	52.5	9.9	2.0	35.6
IPSL-CM5B-LR	1.08	0.13	0.0	80.0	0.0	20.0
MIROC5	19.53	8.68	21.6	0.0	78.4	0.0
MPI-ESM-LR	10.68	4.60	91.3	0.0	8.2	0.0
MPI-ESM-MR	15.25	7.45	88.6	0.0	11.4	0.0
MRI-CGCM3	26.65	16.55	1.1	98.6	0.0	0.0
BNU-ESM	0.28	0.00	0.0	100.0	0.00	0.00
CanESM2	0.24	0.03	100.0	0.0	0.00	0.00
CCSM4	0.00	0.00	…	…	…	…
CESM1-BGC	0.46	0.00	100.0	0.0	0.00	0.00
CESM1-CAM5	0.00	0.00	…	…	…	…
CESM1-WACCM	0.00	0.00	…	…	…	…
CSIRO-Mk3.6	1.97	0.05	56.1	9.9	34.01	0.00
INMCM4	0.00	0.00	…	…	…	…
MIROC-ESM	0.00	0.00	…	…	…	…
MIROC-ESM-CHEM	0.00	0.00	…	…	…	…
NorESM1-M	0.03	0.00	0.0	100.0	0.00	0.00
NorESM1-ME	0.00	0.00	....	…	…	…

Table 2.1: Convection areas in historical (1860-2005) simulations of 36 CMIP5 models. Given are the total circumpolar maximum and mean convection areas (55°S-90°S) as well as the percentage of the mean convection areas found in the Atlantic (65°W-20°E), Indian (20°E-150°E), Western Pacific (210°W-130°W) and Eastern Pacific (130°W-65°W) sectors of the Southern Ocean. The bottom 12 models, featuring no significant open ocean convection, are those that do not simulate any convection area above the 100,000 km^2 threshold (with the exception of CSIRO-Mk3.6, which displayed only one such convective year). The top 24 models are those referred to as 'convecting' models while the bottom 12 models are 'non-convecting' models.

---

to reach about 8.5 $W.m^{-2}$ in 2100, and increases for another 150 years in the 22nd and 23rd century extension, stabilizing after 2250 at approximately 12 $W.m^{-2}$ [Meinshausen *et al.*, 2011]. Note that 'historical' and 'rcp85' simulations analyzed here do not incorporate an interactive carbon cycle.

From monthly salinity and temperature fields, we determined mixed layer depths as the depth z at which $\sigma_\theta(z) - \sigma_\theta(10\ m) = 0.03\ kg.m^{-3}$ [de Boyer Montégut *et al.*, 2004], where σ_θ is the potential density referenced to the surface. This criterion was found to provide a robust diagnostic of modeled mixed layers in the southern polar regions: deep mixed layers were observed to coincide closely with positive sea surface temperature and sea surface salinity anomalies, as well as low sea ice concentration anomalies, signalling the strong vertical flux of heat and salt. In contrast, the Levitus criterion ($\sigma_\theta(z) - \sigma_\theta(0\ m) = 0.125\ kg.m^{-3}$) led to clearly overestimated mixed layer depths in the weakly stratified Southern Ocean. Next, we define a convection area as the total surface area south of 55ºS with a September mixed layer depth exceeding 2000 m. This depth criterion ensures that only deep convection in the open ocean is taken into account. Convection areas are relatively insensitive to the chosen depth threshold because deep convective overturning was generally observed to extend down to the seafloor. September was chosen because maximum convection depths and areas are commonly found at the end of austral

winter. Convective years refer to model years where the convection area is larger than 100,000 km^2, or about a third of the observed 1970s Weddell Polynya area.

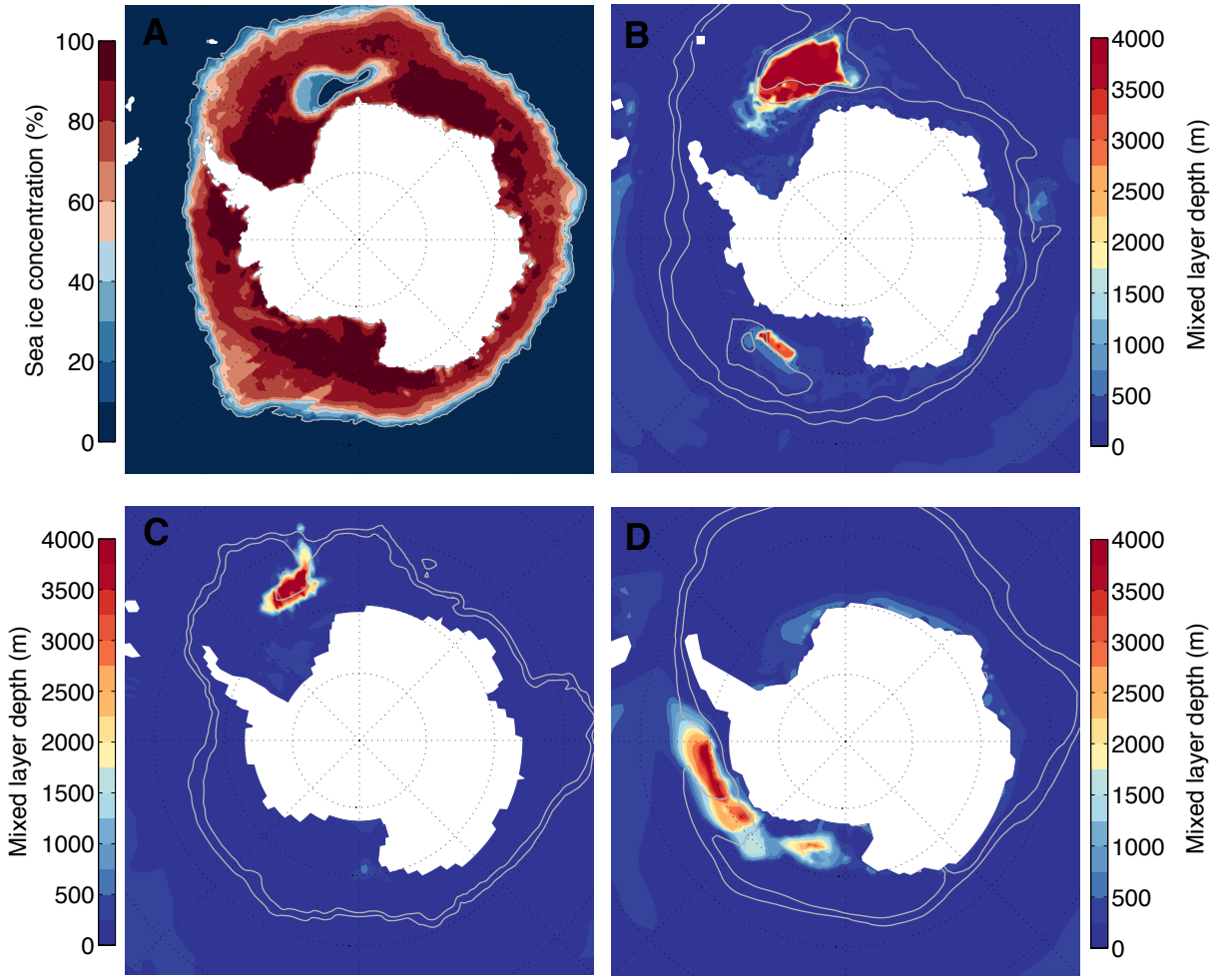

Figure 2.1: Spatial pattern of Southern Ocean deep convection in observations and models. **A,** Observed 1974-1976 mean September sea ice concentration (%) from Nimbus-5 ESMR Polar Gridded Sea Ice Concentrations [Parkinson *et al.*, 1999] delineating the 1974-1976 Weddell Polynya extent. **B,** September mixed layer depth (shading) and 10% and 50% September sea ice concentration contours (light grey lines) in the MPI-ESM-LR model, averaged over years 1886-1888 of the historical simulation. Years presented correspond to the largest three-year-average convection area simulated by MPI-ESM-LR, for illustrative purposes. **C,** Same as **B** for the HadGEM2-ES model, years 1869-1871. **D**, Same as **B** for the IPSL-CM5A-LR model, years 1860-1862. Models chosen because of accurate simulation of bottom water properties and extended RCP8.5 integrations (continuing to year 2300).

2.2 Convection characteristics in CMIP5 models

Two thirds of the models were found to display significant deep (> 2000 m) open ocean convection between 90°S-55°S during more than one year of the historical period (1860-2005). The areal extent of convection averages 860,000 km^2 over 1860-2005 across these 24 models. The Weddell and Ross Gyres generally host most of the deep convection, but some models also place deep convective chimneys in the Indian and Eastern Pacific sectors (Table 2.1). For illustrative purposes, Figure 2.1 shows the spatial pattern of the largest convection events simulated by three models, along with the satellite observations of the 1974-1976 polynya. These three models were chosen because of their relatively accurate simulations of AABW properties and their extended integrations (continuing to year 2300). In the first two models, MPI-ESM-LR and HadGEM2-ES, deep mixed layers, coinciding with anomalously low sea ice concentrations, are found over an area of comparable size to the Weddell Polynya and in a similar location (Figure 2.1 A,B,C). IPSL-CM5A-LR, on the other hand, simulates convection preferentially in the Bellingshausen and Amundsen Seas (Figure 2.1 D, Table 2.1).

The frequency of convective events is highly variable across models (Figure 2.2 and Table 2.2), reflecting the sensitivity of convection to subtle features of ocean circulation, air-sea fluxes, sea ice, and numerical approximations. Eleven of the models simulate convection almost every winter, whereas more than 90 years can separate convective events in some weakly convecting models. The thirteen models that allow only intermittent convection show a mean duration of convective periods ranging between one and 27 years, and a mean hiatus between events of three to 53 years. By averaging over the 24-model ensemble, we find that 65% of all model years exhibit deep convection in the Southern Ocean, with a mean spacing between convective events of 8 years.

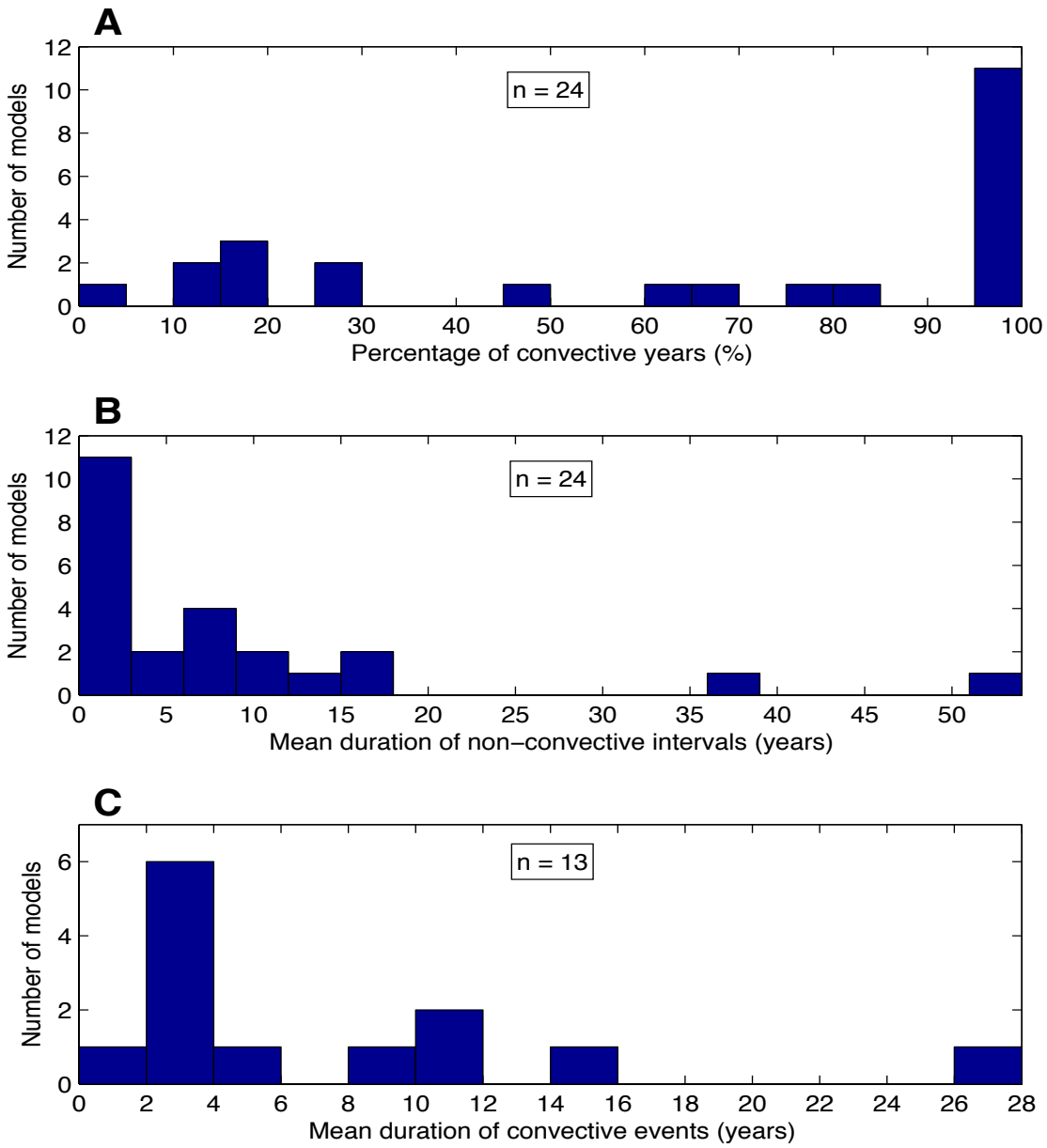

Figure 2.2: Frequency and duration of simulated Southern Ocean convective events. Distribution of the 24 convecting CMIP5 models according to percentage of convective years (**A**) and mean duration of non-convective intervals (**B**), and distribution of 13 intermittently convecting CMIP5 models according to duration of convection events (**C**). The percentage convective years (**A**) is based on the historical period (1860-2005) only, while the lengths of convective (**C**) and non-convective (**B**) intervals are based on the period extending from 1860 to the last convective year simulated by each model. Note that both the frequency and the duration of convective events are highly variable across models. Eleven models simulate convection almost every year.

Models	Percentage convective years (%)	Mean length of convection events (years)	Mean length of non-convective intervals (years)	Length of longest non-convective interval (years)
ACCESS1.0	100.0	…	0.0	0
ACCESS1.3	97.0	…	2.0	3
BCC-CSM1.1	63.0	4.9	3.1	11
BCC-CSM1.1m	81.0	26.8	6.0	25
CMCC-CM	69.0	15.3	6.1	13
CMCC-CMS	30.0	3.8	8.2	39
CNRM-CM5	18.0	9.3	36.0	61
FGOALS-g2	14.0	2.4	11.6	70
FGOALS-s2	100.0	…	0.0	0
GFDL-CM3	77.0	11.9	3.6	7
GFDL-ESM2G	100.0	…	0.0	0
GFDL-ESM2M	97.0	…	0.0	4
GISS-E2-H	100.0	…	0.0	0
GISS-E2-R	100.0	…	0.0	0
HadGEM2-AO	14.0	2.4	14.3	43
HadGEM2-CC	28.0	2.7	7.1	20
HadGEM2-ES	15.0	3.0	15.7	33
IPSL-CM5A-LR	17.0	3.8	16.0	92
IPSL-CM5A-MR	48.0	11.1	10.0	18
IPSL-CM5B-LR	1.0	1.0	53.0	89
MIROC5	100.0	…	0.0	0
MPI-ESM-LR	98.0	…	1.0	1
MPI-ESM-MR	100.0	…	0.0	0
MRI-CGCM3	100.0	…	0.0	0

Table 2.2: Temporal characteristics of convection in 24 convecting CMIP5 models. Convective years correspond to a convection area in excess of 100,000 km^2. The percentage convective years (first column) is based on the historical period (1860-2005) only. The lengths of convective and non-convective intervals are based on the period extending from 1860 to the last convective year simulated by each model.

It is important to bear in mind that these global climate models are too coarsely-resolved to capture the export of shelf waters in downslope currents, and therefore miss this important source of deep ocean ventilation [Heuzé *et al.*, 2013]. The lack of AABW production on shelves could cause the deep Southern Ocean to

be relatively unstratified, making it more prone to convective activity. As a result, the simulated convection may be unrealistically strong in many cases, a behaviour possibly amplified by convective parameterizations necessitated by the coarse resolution, hydrostatic framework of CMIP5 [Kim and Stössel, 2001]. On the other hand, models which do not produce AABW through open ocean convection tend to display larger biases in the properties of AABW than models convecting in the subpolar gyres [Heuzé *et al.*, 2013]. In addition, we show that the twelve models with no significant convective activity over the full simulations have overly-strong vertical stratification, excessive summer ice coverage, or both (Figure 2.3). While a strongly stratified deep ocean can efficiently oppose deep convective mixing, an overestimated summer ice cover, acting as an insulating lid, may impede the formation of a sensible heat polynya and the onset of convection in austral fall. The fact that convective chimneys have been clearly observed in the Weddell Sea [Gordon, 1978; Gordon, 1982; Killworth, 1983; Martinson, 1991] implies that the non-convecting models are missing a real mode of Southern Ocean ventilation. Thus, we view the convecting models as simulating an important pathway of AABW production, albeit often too strongly or sometimes too weakly, depending on the model.

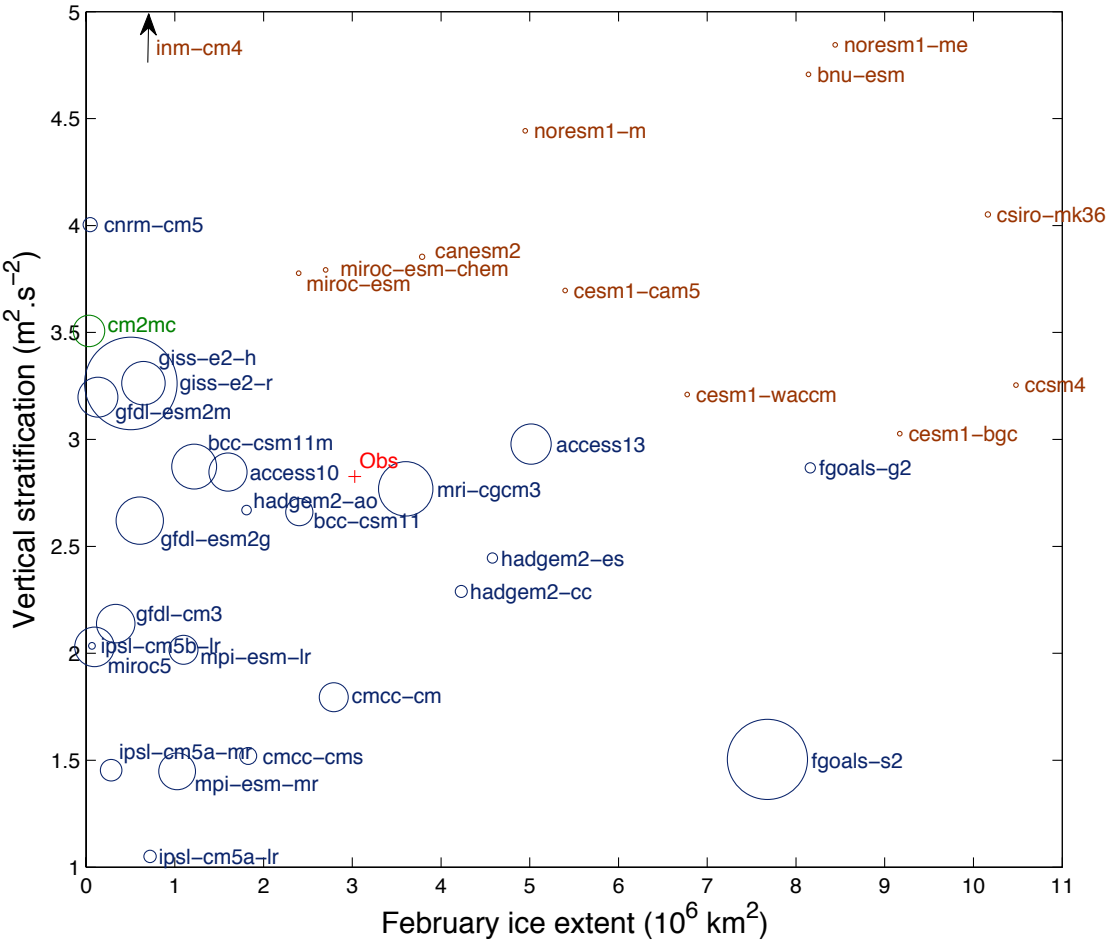

Figure 2.3: Vertical stratification versus February ice extent in the CMIP5 model suite for the 1976-2005 period. Historical mean areal extent of convection reflected by the size of the circle for each model. Vertical stratification is measured by the buoyancy loss necessary for convection to reach a depth of 3000 m in September, calculated as $\frac{g}{\rho_0}\int_0^{3000}\left[\sigma_\theta(3000m)-\sigma_\vartheta(z)\right]dz$, averaged over 55°S-90°S; σ_θ is the potential density referenced to the surface, and g, ρ_0 are constants. Sea ice extent refers to the area where the sea ice concentration is larger than 15 %. All model variables are averaged over 1976-2005. A corresponding observational estimate (red cross) is indicated, where the vertical stratification is calculated from objectively analyzed fields of the World Ocean Atlas 2009 [Locarnini *et al.*, 2010; Antonov *et al.*, 2010] austral winter climatology and the observed February sea ice extent is the 1979-2005 average (data from the National Snow and Ice Data Center [Fetterer *et al.*, 2002]). The 12 models with no significant convective activity over the full simulations (brown) tend to have either strong vertical stratification or large summer sea ice coverage or a combination of both relative to observations. The CM2Mc model (three-member ensemble) is shown in green.

Chapter 3

Response of open ocean convection to anthropogenic climate change

A striking feature emerges from the group of convecting models when they are subjected to increasing CO_2 concentrations following the RCP8.5 scenario: most show a marked decrease in the strength of deep convection over the course of the 20th and 21st centuries (Figure 3.1), with seven models displaying no convective activity after 2030 (see Figure 3.6). Simulations carried out to year 2300 show no return of deep convection over this period, despite the stabilization of atmospheric pCO_2 during the 23rd century. The only model (GISS-E2-R) showing robust convection until 2300 also features the most extensive convection area and poorly represents the meridional water mass structure in the Southern Ocean [Meijers *et al.*, 2013]. To illustrate the variability of convection strengths and the variety of responses across models, we depict time series of the September convection area in the three example models (Figure 3.1 B). Convection weakens and ceases in all three models, although only after 2100 in IPSL-CM5A-LR, which also displays a long hiatus period between 1870 and 1960. The fact that the slowing of Southern Ocean ventilation is so common across models suggests that a relatively simple process is hampering the development of deep convective chimneys under warming conditions.

The high latitude Southern Ocean tends to be destabilized by the presence of relatively warm waters under a cold surface, but this is counteracted by the low salinity of surface waters, maintained by a delicate balance of ocean-ice-atmosphere feedbacks [Martinson, 1991]. Weddell Sea convection is thought to occur when an anomalous salt input to the surface layer triggers an instability. Such destabilizing forcing may result from the advection of a high salinity anomaly into the Weddell Gyre [Galbraith *et al.*, 2011], from low-frequency variability in precipitative-evaporative fluxes related to the Southern Annular Mode [Gordon *et al.*, 2007], or

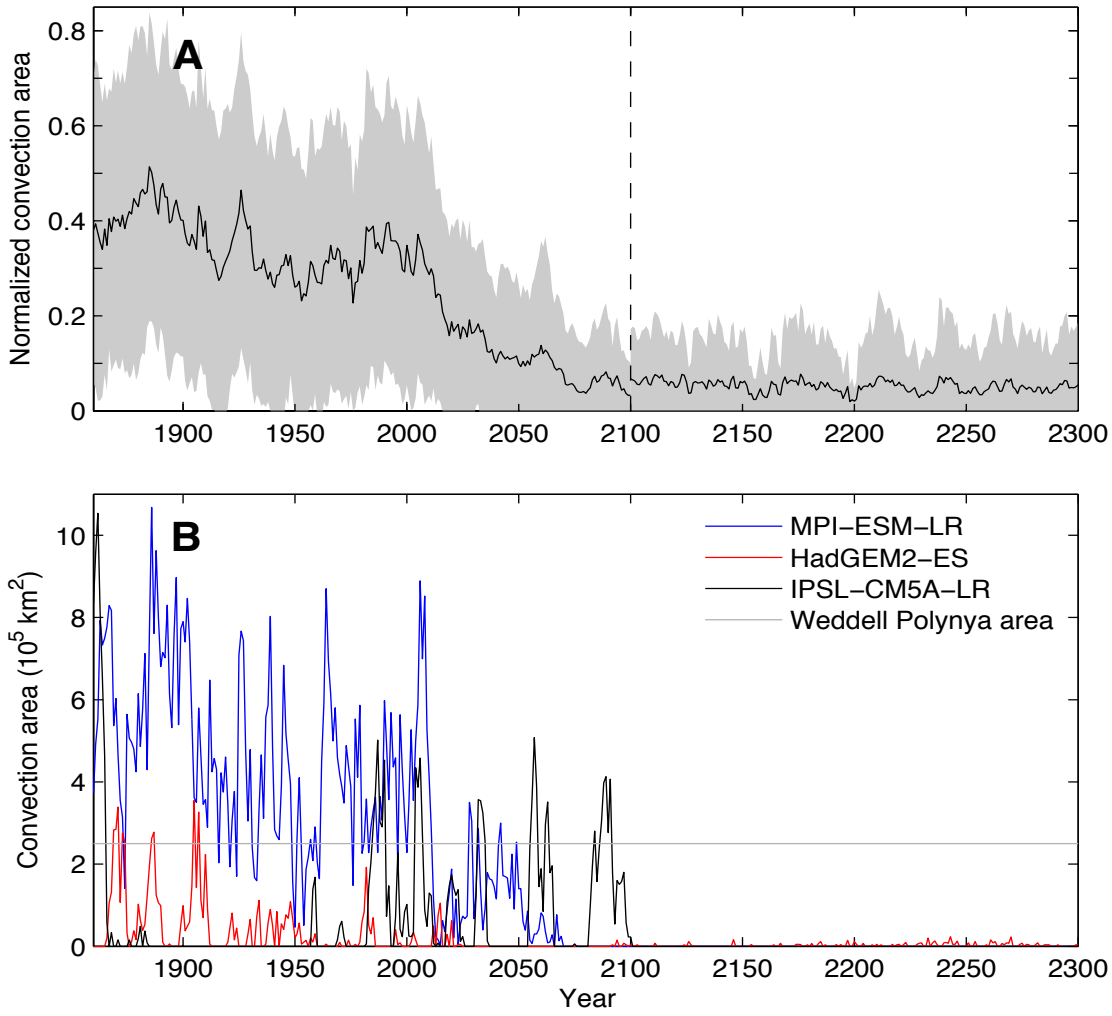

Figure 3.1: Southern Ocean (55°S-90°S) convection area. **A,** Ensemble mean (black line) and multi-model standard deviation (gray shading) of normalized convection areas. 24 CMIP5 convecting models are included. For each model, the area is normalized by the maximum areal extent of convection recorded in the entire simulation. Only seven models are run beyond year 2100. The only model with robust convection until 2300 (GISS-E2-R) also features the most extensive convection area (Table 2.1 and Figure 2.3). **B,** Convection area in the MPI-ESM-LR (blue), HadGEM2-ES (red) and IPSL-CM5A-LR (black) models. The Weddell Polynya area [Carsey, 1980] is indicated by the light grey line for comparison.

from circulation-topography interactions associated with Maud Rise [Gordon *et al.*, 2007; Holland, 2001]. In particular, flow transients upstream of Maud Rise may enhance the local upwelling of salty subsurface waters [Gordon *et al.*, 2007] or initiate a polynya dynamically through the shedding of a large ocean eddy [Holland,

2001]. Brine rejection during sea ice formation also participates in reducing the buoyancy of the mixed layer [Martinson *et al.*, 1981]. Thermobaric effects, arising from the pressure- and temperature-dependence of seawater's thermal expansion coefficient, abruptly extend the depth of convective overturning once it begins, by causing the cold surface waters to become relatively denser as they sink [Killworth, 1979; Akitomo, 1999]. Convection may continue until an excessive surface freshwater supply [Martinson *et al.*, 1981] or the exhaustion of the deep heat reservoir [Martin *et al.*, 2012] allows sea ice to expand and the surface to re-stratify.

To explore the mechanisms driving the shutdown of convection under RCP8.5, we performed additional climate change experiments with a model (CM2Mc) featuring strong, episodic Weddell Sea ventilation events [Galbraith *et al.*, 2011]. The model is a coarse resolution version of NOAA's GFDL coupled climate model, ESM2M [Dunne *et al.*, 2012; see appendix A for a detailed model description]. As described in Bernardello *et al.* [submitted to *Journal of Climate*], the experiments use the historical and RCP8.5 forcing data recommended by the Coupled Model Intercomparison Project-CMIP5, so that the boundary conditions are identical to those used in 'historical' and 'rcp8.5' CMIP5 experiments. Three ensemble members are run, with each member started from initial conditions taken 20 years apart from a 1000-year preindustrial simulation segment performed after the end of the spin-up period.

Convection was found to cease abruptly in all three simulations, with the final convection events ending in years 1952, 1987 and 2005, thus highlighting the sensitivity of the convection cycles to initial conditions. Enhanced freshwater input at southern high latitudes, driven by increased precipitation and decreased evaporation south of 45°S (Figure 3.2), contributes to isolating the surface layer by making it more buoyant and less prone to mixing with underlying saltier waters.

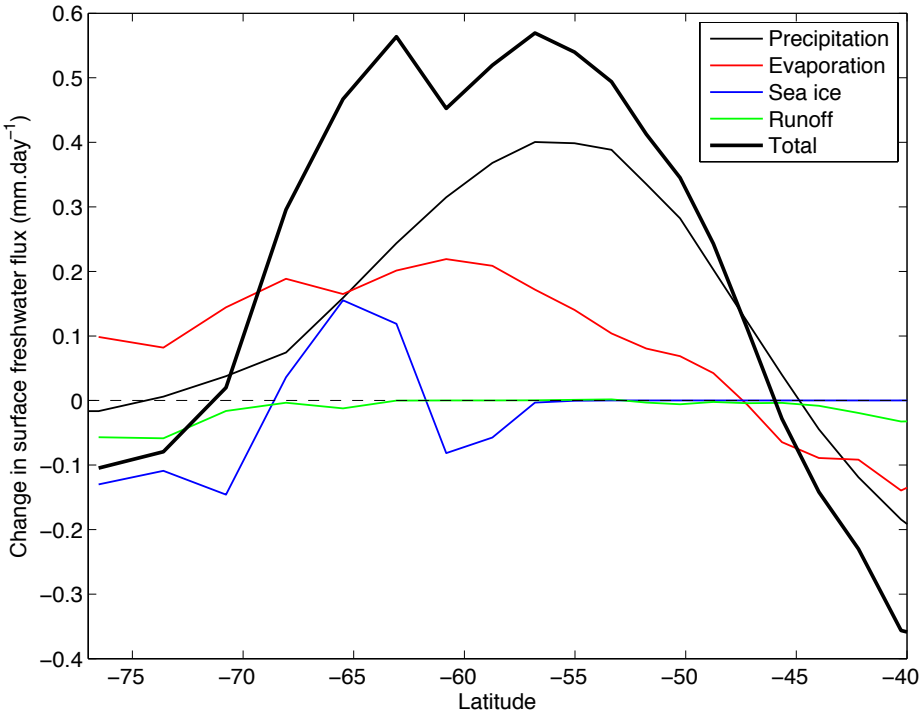

Figure 3.2: Changes in surface freshwater fluxes (mm.day^{-1}) in the CM2Mc climate change model simulations. Zonal mean total change (thick black line) and contributions due to precipitation (black), evaporation (red), sea ice (blue) and runoff (green). Positive values correspond to an increase in freshwater input to the surface ocean. Ensemble multi-annual mean of three simulations presented for years 2070-2100 minus 1860-1890 (the same quantity calculated in pre-industrial control simulations showed the model drift to be negligible). Precipitation and evaporation freshening changes dominate between 71°S and 46°S.

The freshwater gain strengthens the surface stratification, providing an efficient barrier to convective mixing. We note that the change in the precipitation-evaporation balance observed in CM2Mc is qualitatively consistent with an amplification of the global water cycle, related to the ability of warmer air to hold more moisture, and with a southward shift and intensification of extratropical storm tracks in the Southern Hemisphere (Figure 3.3), both well-documented in observations and models [Yin, 2005; Liu and Curry, 2010; Durack *et al.*, 2012; Fyfe *et al.*, 2012].

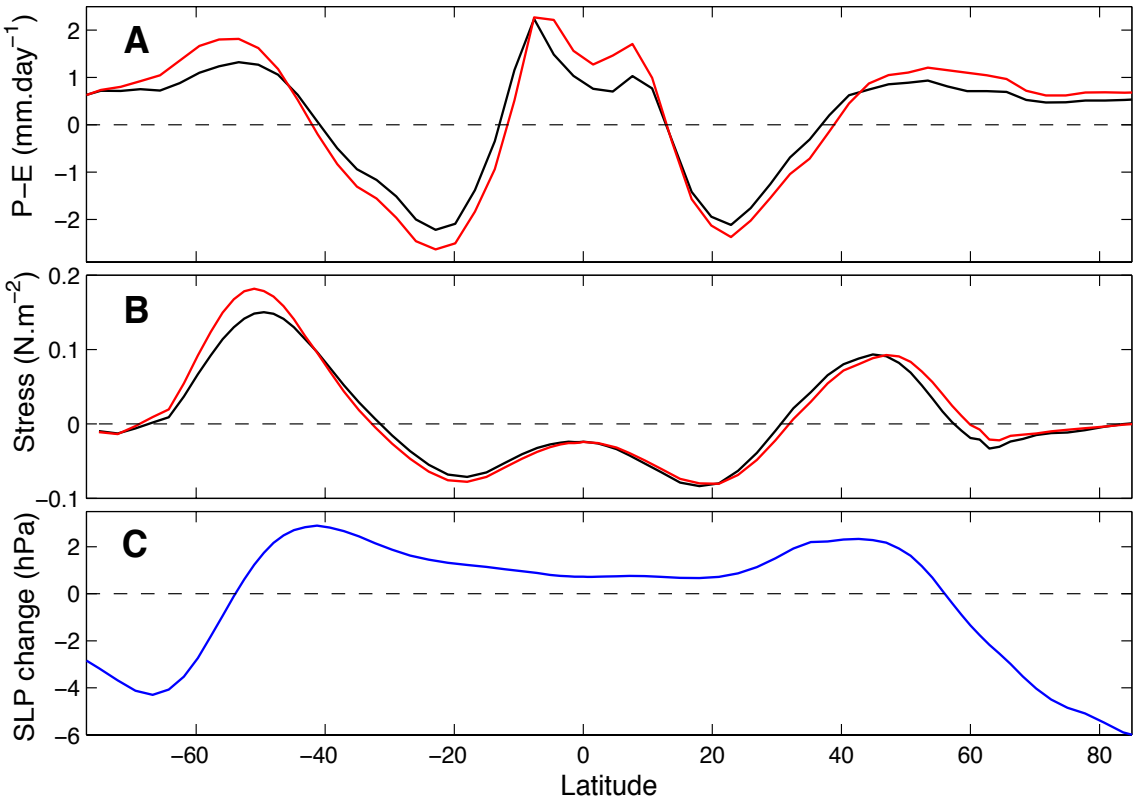

Figure 3.3: Changes in hydrological cycle and low-level atmospheric circulation in the ensemble of CM2Mc climate change simulations. Zonal mean precipitation minus evaporation (P-E) (**A**) and zonal wind stress (**B**) averaged over years 1860-1890 (black) and 2070-2100 (red). Difference in zonal mean sea level pressure (SLP) between years 2070-2100 and 1860-1890 (**C**). The P-E meridional gradients deepen and the high-latitude maxima in P-E shift poleward (**A**). The deepening of the meridional gradient in SLP at about 50°S signals the long-term trend towards higher values of the Southern Annular Mode index (**C**), which is accompanied by a strengthening and southward shift of the low-level atmospheric circulation (**B**).

In order to test the potential importance of wind stress changes on ocean circulation, including long-term trends in the Southern Annular Mode, we made an additional ensemble simulation applying only the wind changes obtained under RCP8.5. To compute the time-varying perturbation to the wind stress, we start by running an additional control simulation, where greenhouse gases are held constant at pre-industrial (1860) levels. We next compute the anomalies in vector wind stress as the differences in monthly means between the climate change and control

simulations. In order to remove the interannual signal caused by the main climate modes of variability, we smooth these anomalies by calculating 20-year running means, for each month, over the period 1860-2100. The smoothed anomalies are then applied at each ocean time step. The wind stress anomalies are applied when the momentum fluxes are passed from the atmosphere to the ocean and do not directly interfere with any other oceanic process. The atmosphere does not feel the wind perturbation except for any feedbacks resulting from changes in ocean circulation, as in Delworth and Zeng [2008]. As evident in Figure 3.4, wind stress changes alone caused no significant decrease in deep Southern Ocean ventilation. Yet, interestingly, the convection shifted from the Weddell Sea to the Ross Sea (not shown).

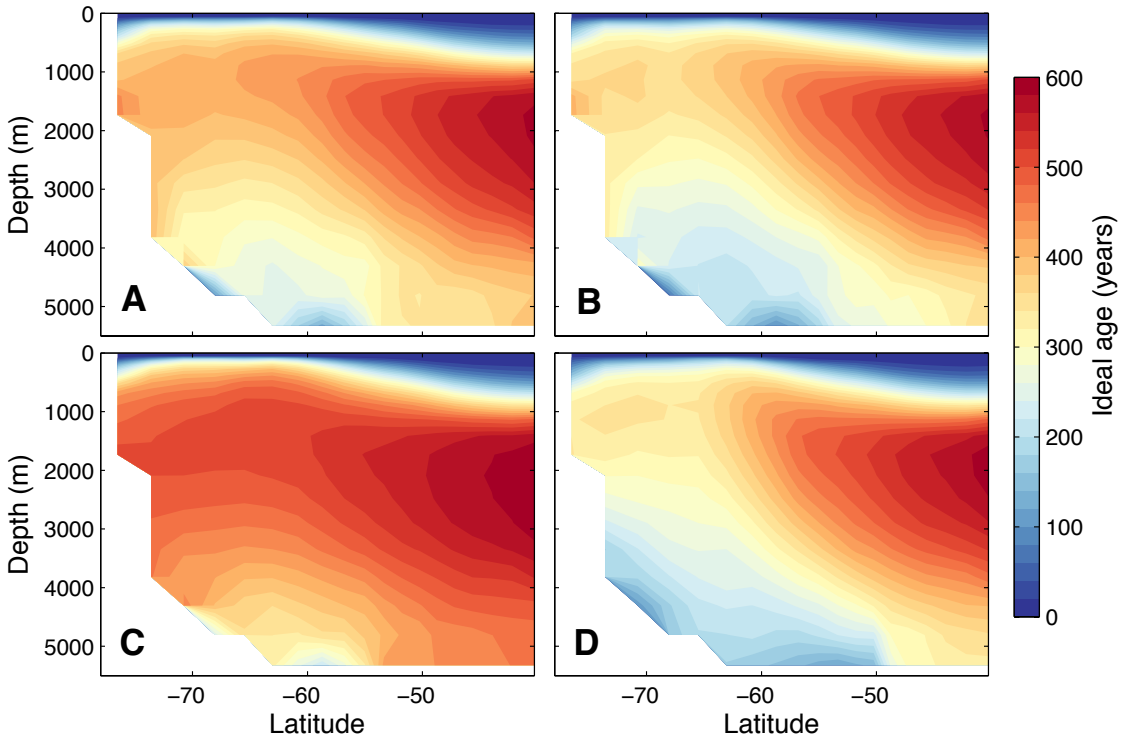

Figure 3.4: Zonal mean water age (since surface contact) in a depth versus latitude Southern Ocean profile for the CM2Mc model. Ensemble mean of three simulations shown for the 1860-1890 and 2070-2100 periods of the climate change simulations (**A** and **C**, respectively) and of the wind-stress perturbation simulations (**B** and **D**). The decrease in ventilation of intermediate and deep waters over 1860-2100 in the climate change experiments is not due to changes in wind stress, and hence must be explained by altered buoyancy fluxes.

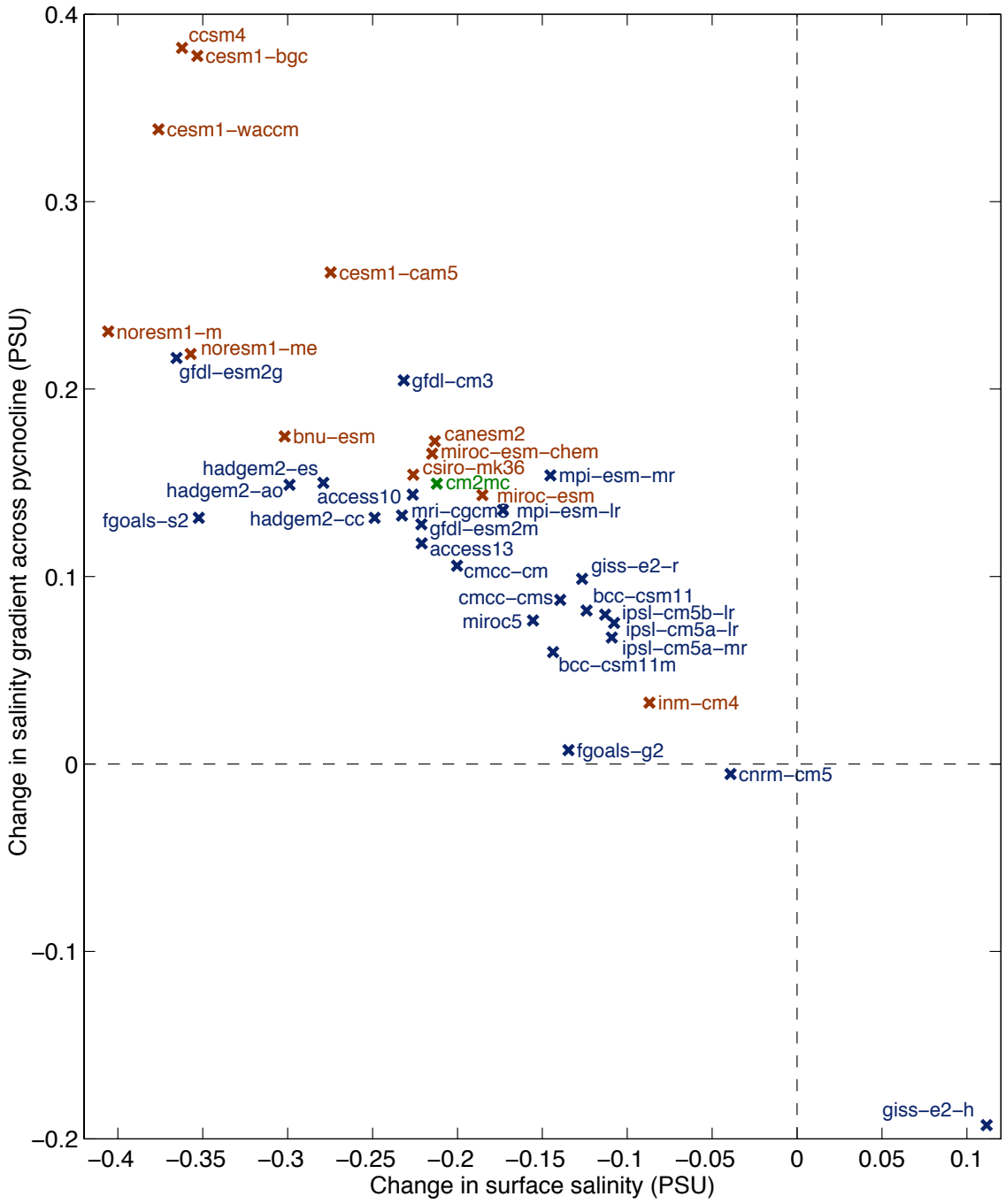

Figure 3.5: Southern Ocean surface salinity changes versus halocline strength changes in the CMIP5 model suite. Variables are September 55°S-90°S averages and changes refer to years 2070-2100 minus 1860-1890 in the RCP8.5 climate change simulations. The halocline strength is calculated as the salinity gradient across the pycnocline (difference between 50 m below and above the depth of maximum stratification). Both convecting (blue) and non-convecting (brown) models are shown. The CM2Mc model ensemble is shown in green.

As in CM2Mc, surface freshening of the high latitude Southern Ocean (55ºS-90ºS) is observed in 35 of the 36 CMIP5 models (Figure 3.5). The resulting increase of salinity stratification causes the pycnocline of all models to strengthen (Figure 3.6). On average, the salinity stratification strengthens later and more slowly in convecting models than in non-convecting models, due to the disruption of freshwater build-up at the surface by convective exchange with saltier deep waters. Moreover, convecting

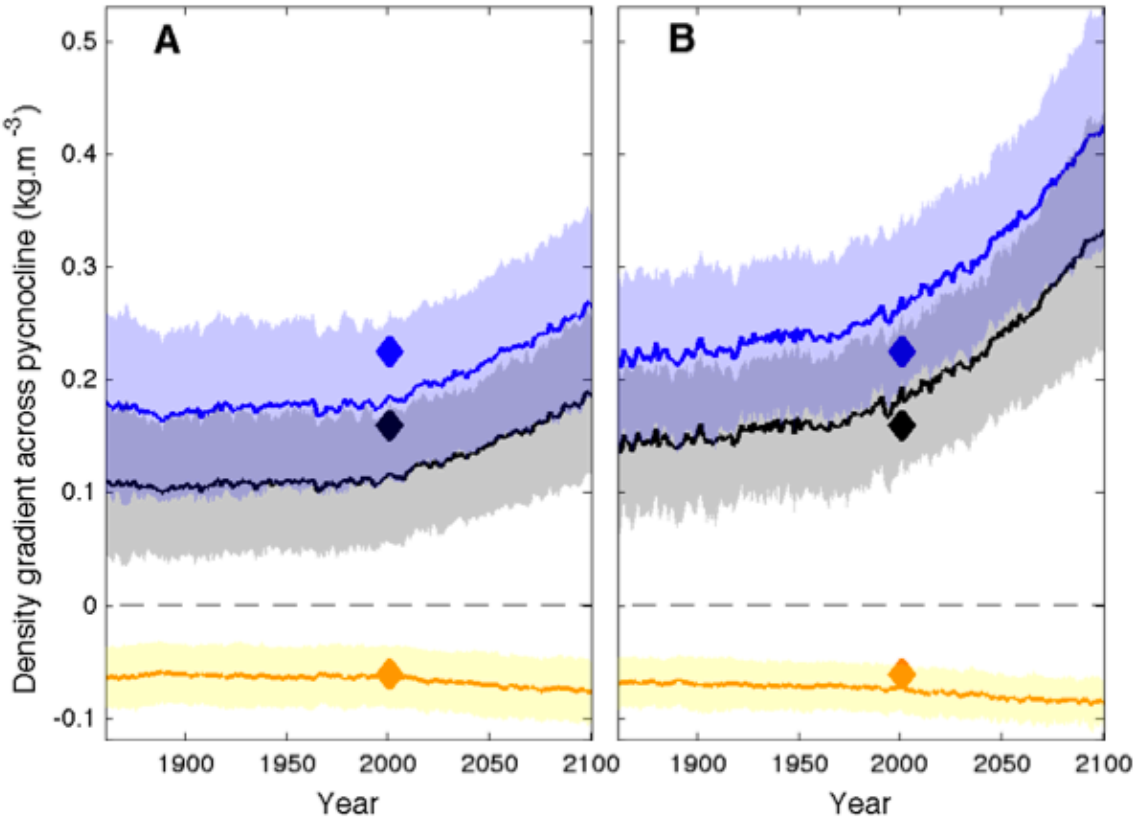

Figure 3.6: Time evolution of high latitude Southern Ocean (55°S-90°S) pycnocline strength for 24 convecting (**A**) and 12 non-convecting (**B**) CMIP5 models run over the 21st century with the RCP8.5 scenario. Ensemble mean of the September density gradient across the pycnocline (difference between 50 m below and above the depth of maximum stratification) ($\Delta\sigma_\theta$, black line) and its temperature ($\frac{d\sigma_\theta}{d\theta}\Delta\theta$, orange) and salinity ($\frac{d\sigma_\theta}{dS}\Delta S$, blue) components. Shadings correspond to one multi-model standard deviation. Corresponding observations from objectively analyzed fields of the austral winter World Ocean Atlas 2009 climatology [Locarnini *et al.*, 2010; Antonov *et al.*, 2010] shown arbitrarily at year 2000 (diamonds).

models tend to have a weaker vertical stability than that estimated from observations, whereas the opposite is true for non-convecting models, consistent with strong surface stratification impeding convection.

Because strong convection slows the surface freshening and acts to maintain the water column in a well-mixed and convection-prone state, the common tendency of convecting models to overestimate convection would be expected to delay their response to a perturbed freshwater balance in comparison with the real ocean. Indeed, models with extensive convection areas generally convect further into the 21st century (Figure 3.7). In addition, we note that CMIP5 models do not include the additional freshwater input from the melting of land-based ice sheets [Helm *et al.*, 2010; Bintanja *et al.*, 2013], and that their CMIP3 predecessors were seen to predict a weaker than observed hydrological cycle intensification during 1950-2000 [Durack *et al.*, 2012]. These climate models thus possibly underestimate the halocline sensitivity to climate warming.

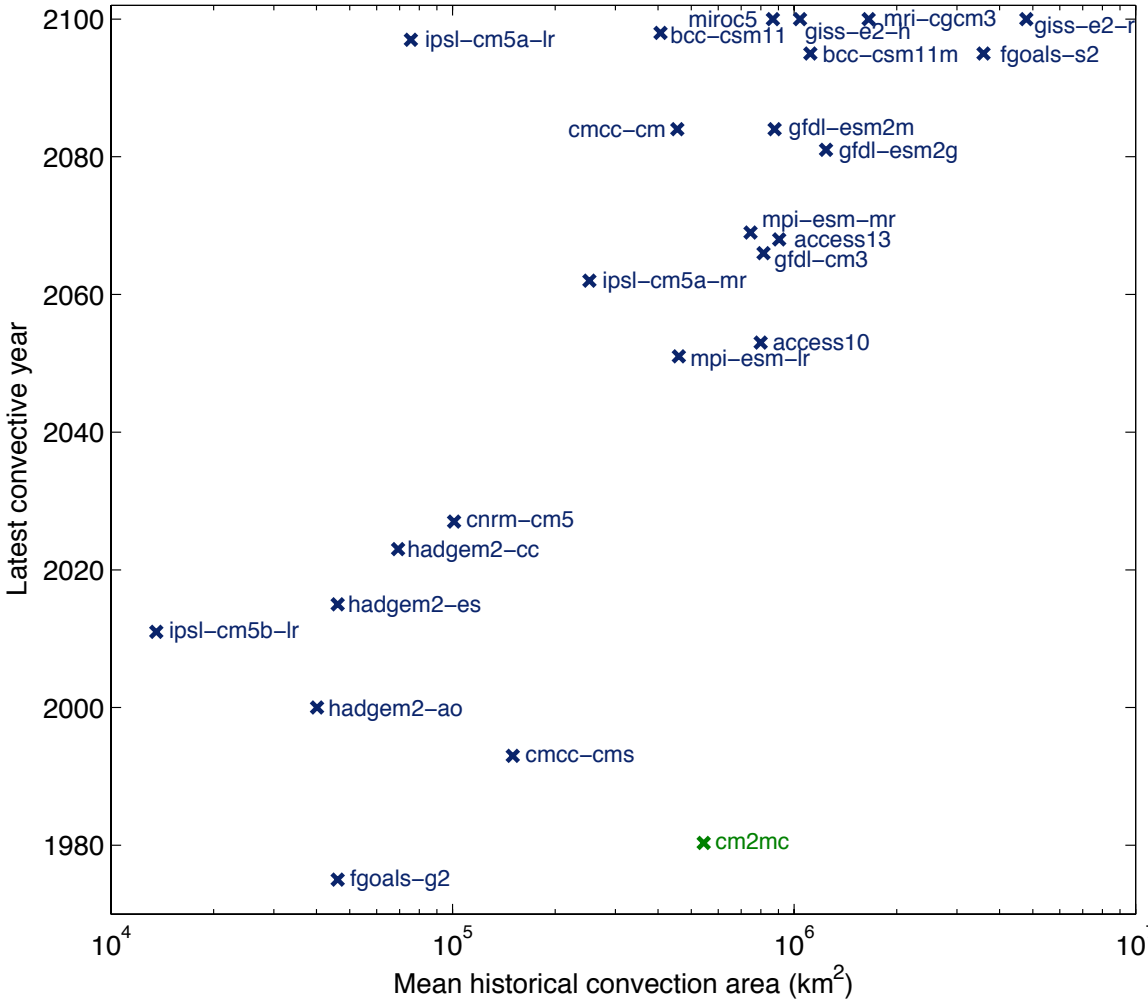

Figure 3.7: Latest convective year versus mean historical convection area in RCP8.5 climate simulations run with the 24 convecting CMIP5 models. Mean historical (1860-2005) area is presented in log scale. The latest convective year corresponds to the last year of the simulation (1860-2100) characterized by a convection area in excess of 100,000 km^2. Note that models with a large mean historical convection area tend to convect further in the 21st century. The three-member CM2Mc ensemble is shown in green.

Chapter 4

Implications for ocean circulation and climate

It is possible that the absence of significant open ocean convection in the Southern Ocean for the past 36 years reflects a natural low frequency of these ventilation events, although a probable Weddell Sea convective event circa 1960 [Gordon, 1982] suggests that a relatively short non-convective interval preceded the 1974-1976 episode. Alternatively, anthropogenic forcing may have already strengthened the Southern Ocean salinity stratification to the point at which convective chimneys are significantly impeded. Indeed, hints of a surface freshening in the Weddell Sea [Gordon *et al.*, 2007; Hellmer *et al.*, 2011] and strong evidence for freshening throughout the Southern Ocean [Durack and Wijffels, 2010], potentially brought on by a persistent positive phase in the Southern Annular Mode [Gordon *et al.*, 2007; Fyfe *et al.*, 2012], global water cycle amplification [Helm *et al.*, 2010; Durack *et al.*, 2012] and ice-shelf basal melting [Bintanja *et al.*, 2013], point to an increase in stability over recent decades. It therefore seems likely that deep convection in the Southern Ocean has already been impacted by anthropogenic climate change.

Given the large amounts of AABW produced during the 1974-1976 event [Gordon, 1982], a decreasing frequency of deep convection would be expected to have caused a significant slowdown in AABW production. The recent absence of Weddell Sea convection could therefore be contributing to the observed warming, salinification [Fahrbach *et al.*, 2011] and aging [Huhn *et al.*, 2013] of Weddell Sea Deep Water, and to the reported warming and volume loss of AABW in the western Atlantic [Coles *et al.*, 1996; Zenk and Morozov, 2007; Johnson *et al.*, 2008; Purkey and Johnson, 2012]. A recent study [Latif *et al.*, in press] suggests that the present

halt of the deep convection, attributed to centennial natural climate variability rather than anthropogenic forcing, could also contribute to recent trends in Southern Hemisphere surface climate. Using a model featuring multi-centennial convection cycles, Latif *et al.* remark that observational trends of the last several decades show numerous similarities with post-convective phases in the model. Indeed, a reduced convective activity is consistent with high latitude surface cooling, deep ocean warming, sea ice expansion and poleward-intensifying surface westerlies, all observed changes in the Southern Ocean region [Latif *et al.*, in press; Purkey and Johnson, 2010; Cavalieri and Parkinson, 2008; Visbeck, 2009]. An analogous climate signature of non-convective periods is seen in CM2Mc (see Appendix B).

A regime shift in Southern Ocean deep ventilation would have also had significant impacts on the air-sea exchange of heat. The heat release from the Weddell Polynya over 1974-1976 was estimated to be about 0.4 x 10^{21} J per year [Gordon, 1982], equivalent to approximately 8% of the average annual rise in ocean heat content over the period 1972-2008 [Church *et al.*, 2011]. Hence, stratification in the Weddell Sea may have already played a significant role as a "heat buffer" [Fahrbach *et al.*, 2011], causing heat to accumulate in the abyss rather than being released by convection. Additionally, by exchanging with the vast deep ocean carbon pool, Weddell convective events modify atmospheric pCO_2 significantly [Bernardello *et al.*, submitted to *Journal of Climate*].

Long-term fluctuations in northern and southern deep water formation rates and associated reorganizations in the meridional overturning circulation have been proposed to play a prominent role in natural climate changes [e.g., Broecker, 1997; Clark *et al.*, 2002]. Changes in ocean heat and carbon storage associated with changes in convective activity in the Southern Ocean may have directly contributed to past regional or global climate variations, such as during the last deglaciation, when proxies suggest marked ventilation changes in the deep South Atlantic [Burke and

Robinson, 2012]. In a more recent past, it is possible that the relatively warm conditions found over the Antarctic continent during the Little Ice Age [Broecker *et al.*, 1999; Broecker, 2000] coincided with vigorous open ocean convection in the Weddell Sea.

APPENDIX

A. Model description

The model used for the additional simulations, CM2Mc [Galbraith *et al.*, 2011], is a three-degree version of NOAA GFDL's coupled climate model, ESM2M [Dunne *et al.*, 2012], without the adaptive land model. CM2Mc uses a similar atmosphere as ESM2M and its progenitor CM2.1 [Delworth *et al.*, 2006], with minor alterations as required to adjust to the coarser discretization. The CM2Mc ocean uses a tripolar grid with enhanced latitudinal resolution near the equator and at mid-latitudes, benefiting the resolution of equatorial currents. There are 28 vertical levels unevenly distributed with a finer resolution towards the surface. Eddy mixing is represented using the parameterization of Gent and McWilliams [1990] with a spatially varying diffusion coefficient [Griffies *et al.*, 2005]. Subgrid-scale oceanic convection is parameterized as part of the surface boundary layer scheme, which uses the K-profile parameterization [Large *et al.*, 1994]. The atmosphere used here employs the M30 grid, with a latitudinal (longitudinal) resolution of 3 (3.75) degrees and 24 vertical levels. As in CM2.1, the CM2Mc land component is the Land Dynamics model of Milly and Schmakin [2002], which includes a river routing scheme but no terrestrial ecosystem.

B. Impact of convective events on climate and ocean circulation in CM2Mc.

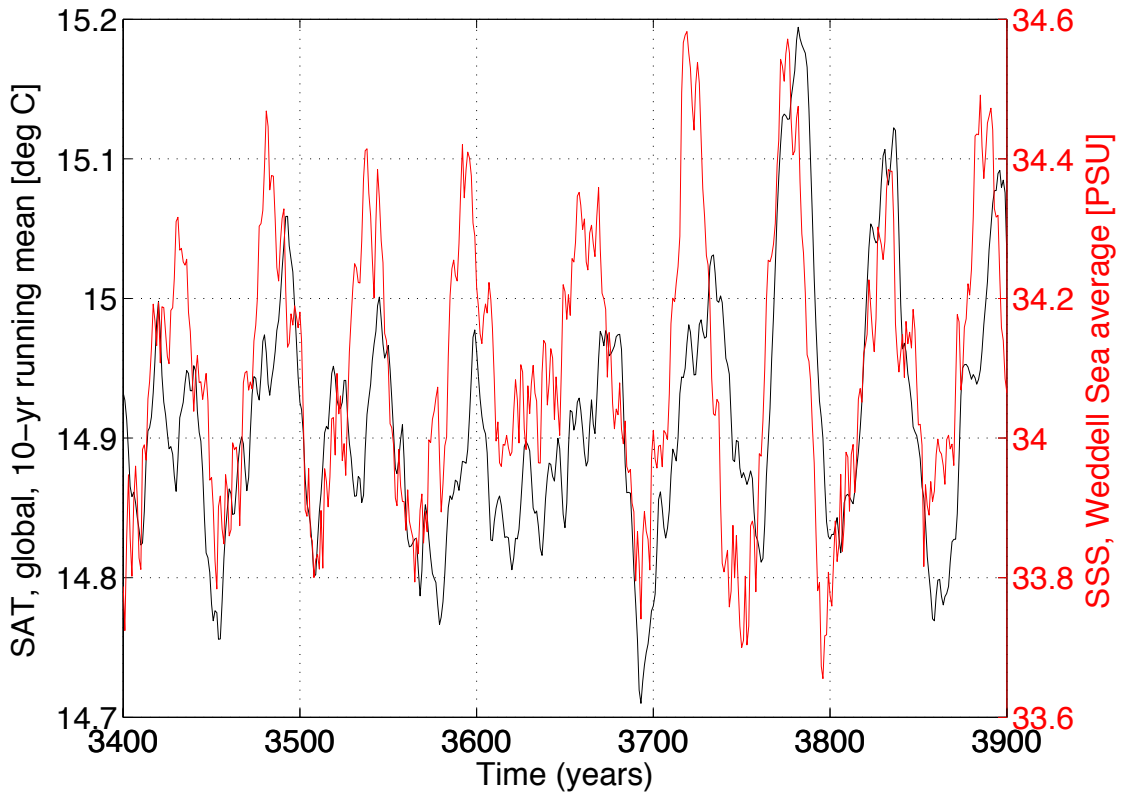

Figure B.1: Evolution of global mean surface air temperature (SAT, black) and Weddell Sea (73°S-68°S; 50°W-30°W average) sea surface salinity (SSS, red) over 500 years of a pre-industrial control simulation. CM2Mc shows very strong multi-decadal variability controlled by Weddell Sea cycles where convective and non-convective states alternate. The periodicity is 55 years on average. Convective events induce a massive heat release from the ocean to the atmosphere, causing the global surface air temperature to rise by 0.2-0.4 °C from through to peak. The maximum correlation is 0.7036 with a lag of +4 years: Weddell Sea surface salinity variations precede variations in global mean surface air temperature.

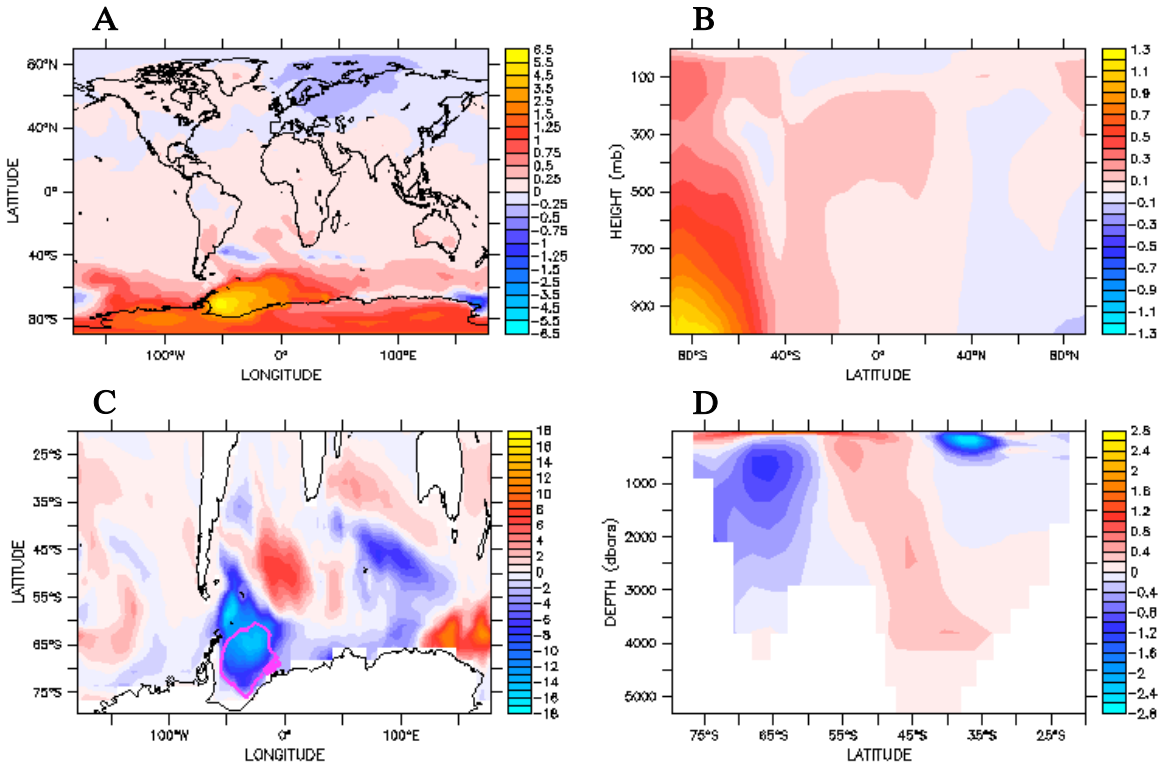

Figure B.2: Climate signature of Weddell Sea convective events in a CM2Mc pre-industrial control simulation. Surface (**A**) and zonal mean (**B**) air temperature anomaly (°C) associated with deep convection, with respect to the non-convective state. **C**, Ocean content change ($GJ.m^{-2}$) induced by convection event (5-year mean following convection minus 5-year mean preceding convection). The pink line encircles the convection area (600 m annual mixed layer contour). **D**, Ocean temperature anomaly (°C) at 40°W associated with deep convection, with respect to the non-convective state. Convective state corresponds to years with a maximum 73°S-68°S; 50°W-30°W annual mixed layer depth greater than 1400 m, whereas non-convective state refers to years with an average 73°S-68°S; 50°W-30°W annual mixed layer depth less than 200 m. Note the strong Southern Hemisphere warming associated with convection and apparent teleconnections with northern Eurasia (**A**). The dipole of ocean temperature anomalies in **D** is due both to convective heat release and southward shift of the Antarctic Circumpolar Current (ACC) compensating for the deep outflow from the Weddell Sea. Note that this cooling/warming dipole results in an increase of the local meridional density gradient and thereby of the ACC transport. Additionally, the warming of the high latitude atmosphere during convection (**A**, **B**) reduces the meridional temperature gradient, weakening the storm tracks [Yin, 2005] and the low-level atmospheric circulation [Latif *et al.*, in press]. (Conversely, note that a convection halt would contribute to a positive trend in the Southern Annular Mode - a potential positive feedback to the surface freshening responsible for convection cessation in climate change simulations.)

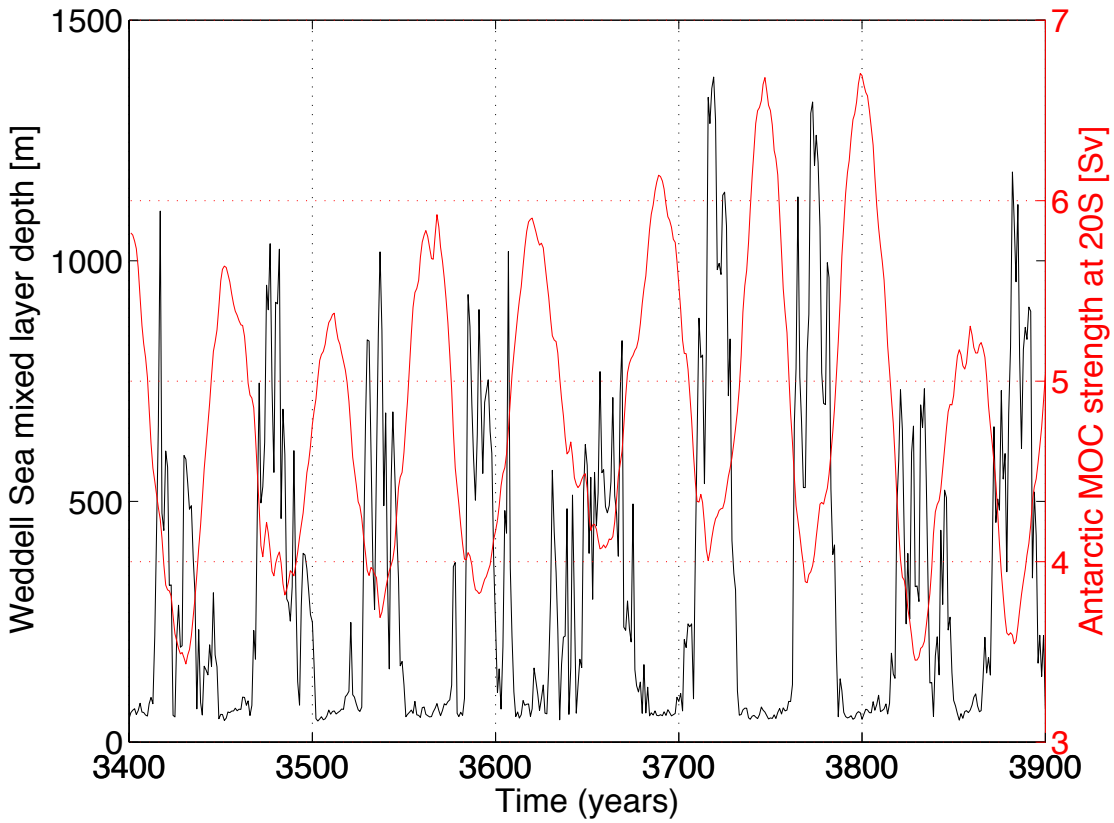

Figure B.3: Evolution of Weddell Sea (73°S-68°S; 50°W-30°W average) annual mixed layer depth (black) and AABW transport at 20°S in the Atlantic (red) over 500 years of a CM2Mc pre-industrial control simulation. AABW transport is calculated as the minimum of the Atlantic meridional overturning streamfunction at 20°S and smoothed with a 10-year running mean. Pulses of Antarctic Bottom Water transport are seen to follow each convection event. The maximum correlation is 0.7486 with a lag of +27 years: it takes about 30 years for most of the deep water formed in the Weddell Sea to be exported to 20°S in the South Atlantic.

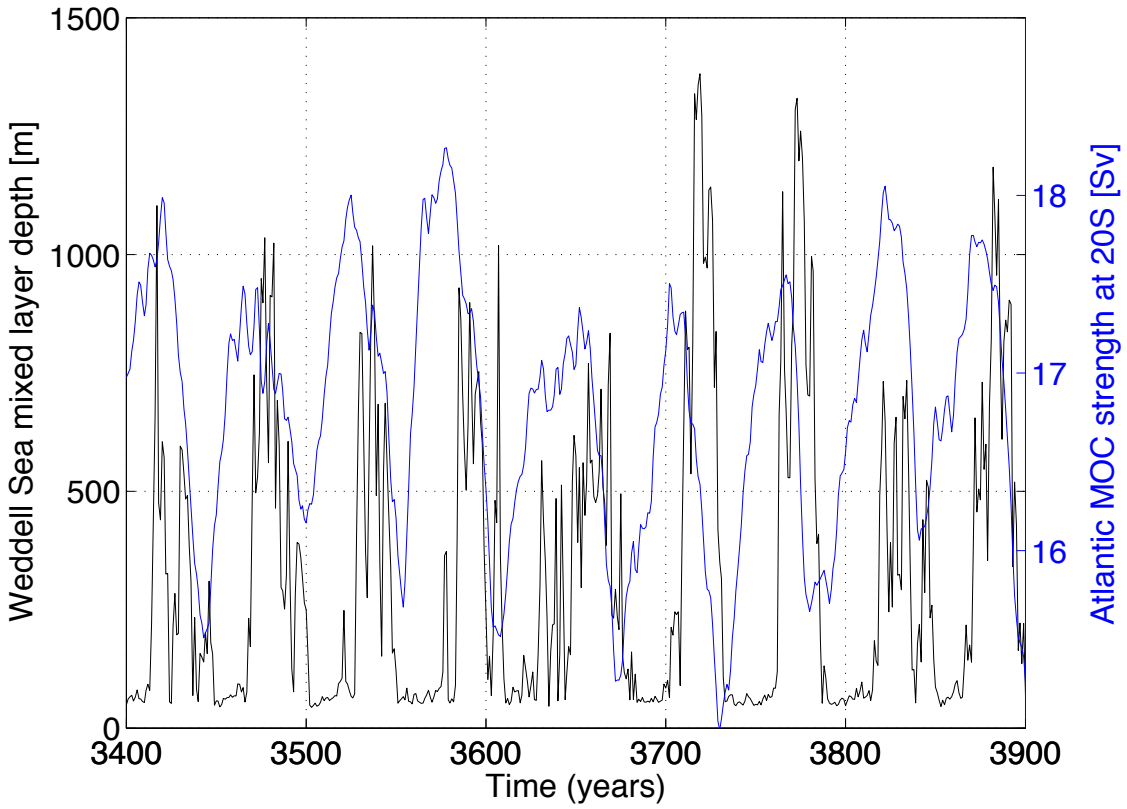

Figure B.4: Evolution of Weddell Sea (73°S-68°S; 50°W-30°W average) annual mixed layer depth (black) and NADW transport at 20°S (blue) over 500 years of a CM2Mc pre-industrial control simulation. NADW transport is calculated as the maximum of the Atlantic meridional overturning streamfunction at 20°S and smoothed with a 10-year running mean. The max correlation is -0.7418, with a lag of + 14 years: a low in NADW transport at 20°S follows a convective event by 14 years. Both upper and lower limbs of the Atlantic meridional overturning respond to Weddell Sea convective events, resulting in a seesaw in AABW and NADW transport (with the minimum in NADW transport leading the maximum in AABW transport by ~13 years). Following convection a large inflow of AABW raises isopycnals in the South Atlantic, increasing the slope of isopycnals and the meridional density gradient, thereby slowing NADW transport [Swingedouw *et al.*, 2009; Martin *et al.*, 2012].

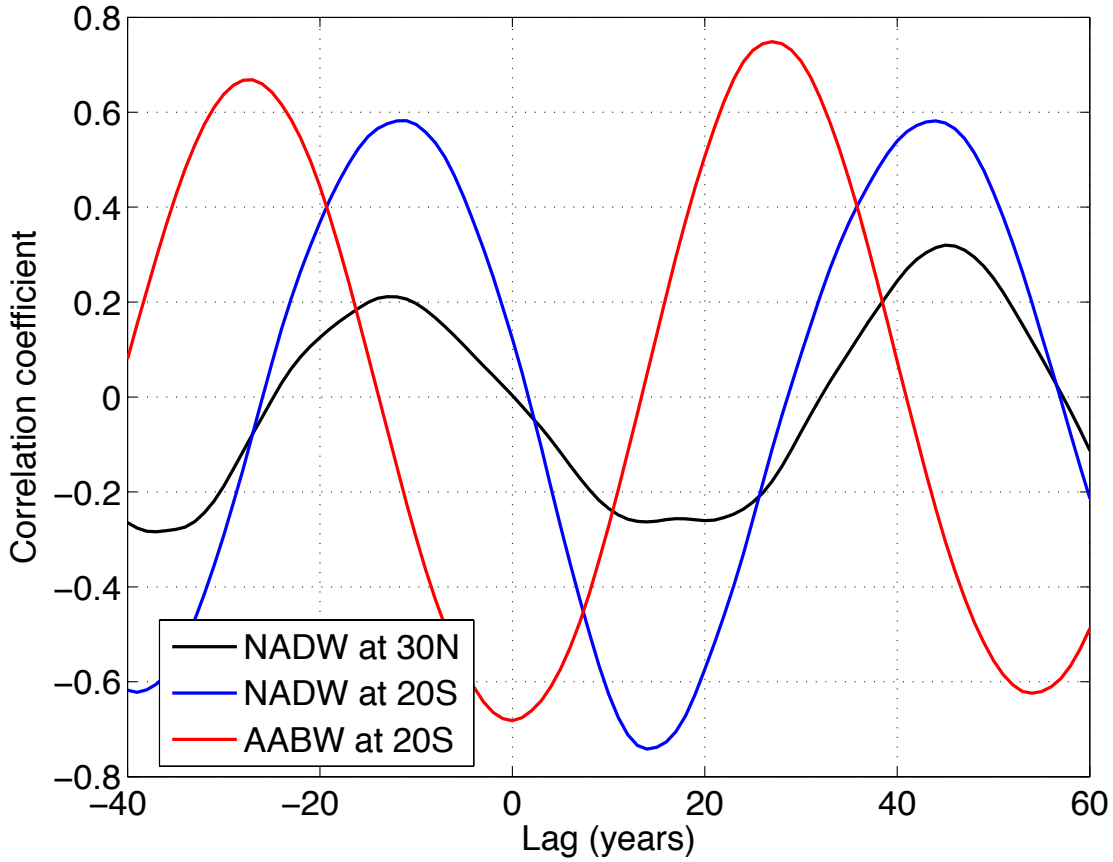

Figure B.5: Correlation between Weddell Sea mixed layer depth (73°S-68°S; 50°W-30°W annual mean average) and Atlantic NADW and AABW transports (10-year running mean) as a function of time lag. As noted in Figure C.3 and C.4, AABW and NADW transports at 20°S correlate best with Weddell Sea convection positively and negatively at lags of +27 and +14 years, respectively. A correlation between NADW transport at 30°N and the Weddell Sea mixed layer is also evident, though weaker. Strong autocorrelation overall compromises reliable time sequence or causation inferences.

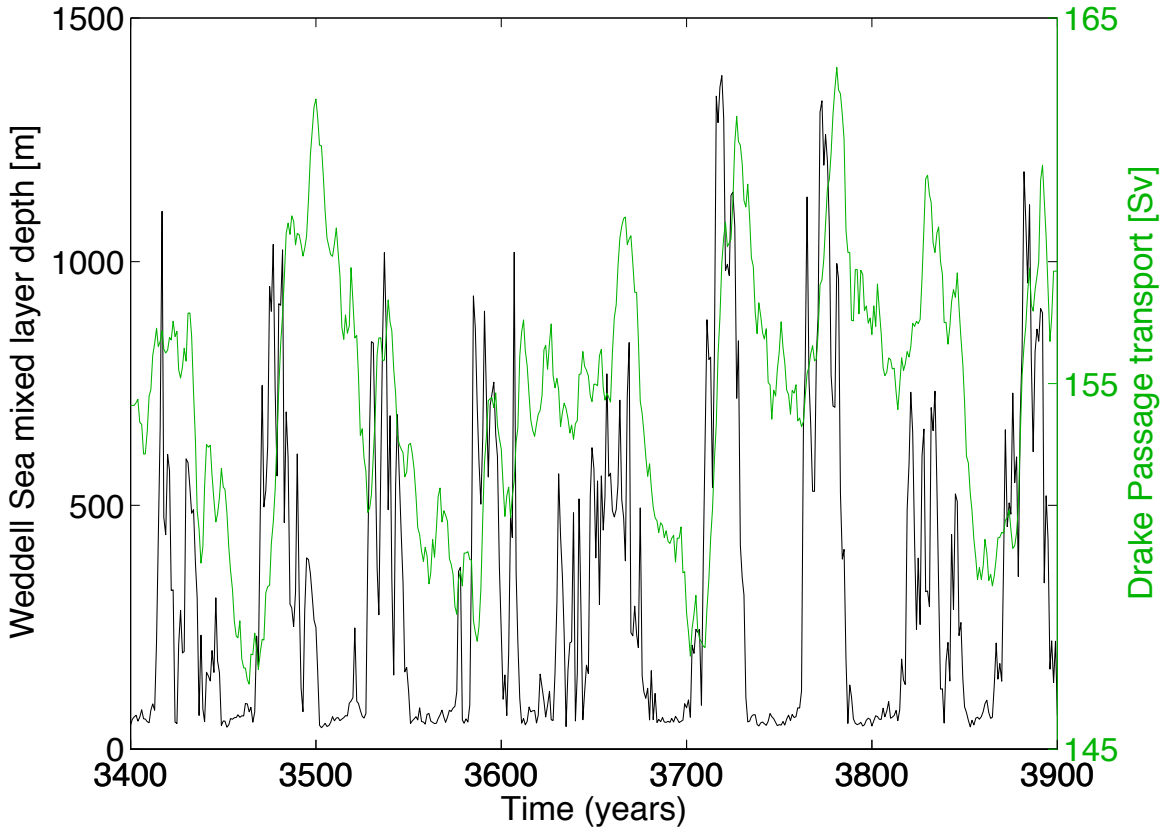

Figure B.6: Evolution of Weddell Sea (73°S-68°S; 50°W-30°W average) annual mixed layer depth (black) and Drake Passage transport (green) over 500 years of a CM2Mc pre-industrial control simulation. Convection produces dense water on the southward edge of the ACC, increasing the local meridional density gradient and thus the eastward geostrophic transport. Note that the ACC intensifies mostly on its poleward side (not shown): the transport increase results essentially from the southward extension and associated widening of the current. The maximum correlation is 0.4880 with a lag of +6 years.

BIBLIOGRAPHY

Akitomo, K. (1999). Open-ocean deep convection due to thermobaricity: 1. Scaling argument. *Journal of Geophysical Research, 104*(C3), 5225-5234.

Antonov, J. I., D. Seidov, T. P. Boyer, R. A. Locarnini, A. V. Mishonov, H. E. Garcia, O. K. Baranova, M. M. Zweng, D. R. Johnson. (2010). *World Ocean Atlas 2009, Volume 2: Salinity.* (Vol. 2). Washington, D.C.: U.S. Government Printing Office.

Bernardello, R., I. Marinov, J. B. Palter, J. L. Sarmiento, E. D. Galbraith, R. D. Slater. Response of the ocean natural carbon storage to projected 21st century climate change, submitted to *Journal of Climate*.

Bintanja, R., G. J. van Oldenborgh, S. S. Drijfhout, B. Wouters, C. A. Katsman. (2013). Important role for ocean warming and increased ice-shelf melt in Antarctic sea-ice expansion. *Nature Geoscience, 6*(5), 376-379.

Broecker, W. S. (1997). Thermohaline Circulation, the Achilles Heel of Our Climate System: Will Man-Made CO2 Upset the Current Balance? *Science, 278*(5343), 1582-1588.

Broecker, W. S. (2000). Was a change in thermohaline circulation responsible for the Little Ice Age? *Proceedings of the National Academy of Sciences, 97*(4), 1339-1342.

Broecker, W. S., S. Sutherland, T-H. Peng. (1999). A possible 20th-century slowdown of Southern Ocean deep water formation. *Science, 286*(5442), 1132-1135.

Burke, A., L. F. Robinson. (2012). The Southern Ocean's role in carbon exchange during the last deglaciation. *Science, 335*(6068), 557-561.

Carsey, F. D. (1980). Microwave Observation of the Weddell Polynya. *Monthly Weather Review, 108*(12), 2032-2044.

Cavalieri, D. J., C. L. Parkinson. (2008). Antarctic sea ice variability and trends, 1979–2006. *Journal of Geophysical Research, 113*(7), C07004.

Church, J. A., N. J. White, L. F. Konikow, C. M. Domingues, J. G. Cogley, E. Rignot, I. Velicogna. (2011). Revisiting the Earth's sea-level and energy budgets from 1961 to 2008. *Geophysical Research Letters, 38*(18), L18601.

Clark, P. U., N. G. Pisias, T. F. Stocker, A. J. Weaver. (2002). The role of the thermohaline circulation in abrupt climate change. *Nature, 415*(6874), 863-869.

Coles, V. J., M. S. McCartney, D. B. Olson, W. M. Smethie Jr. (1996). Changes in Antarctic Bottom Water properties in the western South Atlantic in the late 1980s. *Journal of Geophysical Research, 101*(C4), 8957-8970.

de Boyer Montégut, C., G. Madec, A. S. Fischer, A. Lazar, D. Iudicone. (2004). Mixed layer depth over the global ocean: An examination of profile data and a profile - based climatology. *Journal of Geophysical Research, 109*(C12), C12003.

Delworth, T. L., F. Zeng. (2008). Simulated impact of altered Southern Hemisphere winds on the Atlantic meridional overturning circulation. *Geophysical Research Letters, 35*(20), L20708.

Dunne, J. P., J. G. John, A. J. Adcroft, S. M. Griffies, R. W. Hallberg, E. Shevliakova, ... & N. Zadeh. (2012). GFDL's ESM2 Global Coupled Climate-Carbon Earth System Models. Part I: Physical Formulation and Baseline Simulation Characteristics. *Journal of Climate, 25*(19), 6646-6665.

Durack, P. J., S. E. Wijffels. (2010). Fifty-year trends in global ocean salinities and their relationship to broad-scale warming. *Journal of Climate, 23*(16), 4342-4362.

Durack, P. J., S. E. Wijffels, R. J. Matear (2012). Ocean salinities reveal strong global water cycle intensification during 1950 to 2000. *Science, 336*(6080), 455-458.

Fahrbach, E., M. Hoppema, G. Rohardt, O. Boebel, O. Klatt, A. Wisotzki. (2011). Warming of deep and abyssal water masses along the Greenwich meridian on decadal time scales: The Weddell gyre as a heat buffer. *Deep Sea Research Part II: Topical Studies in Oceanography, 58*(25), 2509-2523.

Fetterer, F., K. Knowles, W. Meier, M. Savoie (2002, updated 2009). Sea Ice Index. Boulder, Colorado USA: National Snow and Ice Data Center.

Fyfe, J. C., N. P. Gillett, G. J. Marshall. (2012). Human influence on extratropical Southern Hemisphere summer precipitation. *Geophysical Research Letters, 39*(23), L23711.

Galbraith, E.D., E. Y. Kwon, A. Gnanadesikan, K. B. Rodgers, S. M. Griffies, D. Bianchi, I. M. Held. (2011). Climate Variability and Radiocarbon in the CM2Mc Earth System Model. *Journal of Climate, 24*(16), 4230-4254.

Gent, P. R., J. C. Mcwilliams. (1990). Isopycnal mixing in ocean circulation models. *Journal of Physical Oceanography, 20*(1), 150-155.

Gordon, A. L. (1978). Deep antarctic convection west of Maud Rise. *Journal of Physical Oceanography, 8*(4), 600-612.

Gordon, A. L. (1982). Weddell deep water variability. *Journal of Marine Research, 40*, 199-217.

Gordon, A. L., M. Visbeck, B. Huber. (2001). Export of Weddell Sea deep and bottom water. *Journal of Geophysical Research, 106*(C5), 9005-9017.

Gordon, A. L., M. Visbeck, J. C. Comiso. (2007). A Possible Link between the Weddell Polynya and the Southern Annular Mode*. *Journal of Climate, 20*(11), 2558-2571.

Griffies, S. M., A. Gnanadesikan, K. W. Dixon, J. P. Dunne, R. Gerdes, M. J. Harrison, ... & R. Zhang. (2005). Formulation of an ocean model for global climate simulations. *Ocean Science, 1*(1), 45-79.

Hellmer, H. H., O. Huhn, D. Gomis, R. Timmermann. (2011). On the freshening of the northwestern Weddell Sea continental shelf. *Ocean Science, 7*(3), 305-316.

Helm, K. P., N. L. Bindoff, J. A. Church. (2010). Changes in the global hydrological-cycle inferred from ocean salinity. *Geophysical Research Letters, 37*(18), L18701.

Heuzé, C., K. J. Heywood, D. P. Stevens, J. K. Ridley. (2013). Southern Ocean bottom water characteristics in CMIP5 models. *Geophysical Research Letters, 40*(7), 1409-1414.

Holland, D. M. (2001). Explaining the Weddell Polynya--a large ocean eddy shed at Maud Rise. *Science, 292*(5522), 1697-1700.

Huhn, O., M. Rhein, M. Hoppema, S. van Heuven. (2013). Decline of deep and bottom water ventilation and slowing down of anthropogenic carbon storage in the Weddell Sea, 1984–2011. *Deep Sea Research Part I: Oceanographic Research Papers, 76*, 66-84.

Johnson, G. C. (2008). Quantifying Antarctic bottom water and North Atlantic deep water volumes. *Journal of Geophysical Research: Oceans, 113*(C5), C05027.

Johnson, G. C., S. G. Purkey, J. M. Toole. (2008). Reduced Antarctic meridional overturning circulation reaches the North Atlantic Ocean. *Geophysical Research Letters, 35*(22), L22601.

Killworth, P. D. (1979). On "chimney" formations in the ocean. *Journal of Physical Oceanography, 9*(3), 531-554.

Killworth, P. D. (1983). Deep convection in the world ocean. *Reviews of Geophysics, 21*(1), 1-26.

Kim, S. J., A. Stössel. (2001). Impact of subgrid-scale convection on global thermohaline properties and circulation. *Journal of Physical Oceanography, 31*(3), 656-674.

Kuhlbrodt, T., A. Griesel, M. Montoya, A. Levermann, M. Hofmann, S. Rahmstorf. (2007). On the driving processes of the Atlantic meridional overturning circulation. *Reviews of Geophysics, 45*(2), RG2001.

Large, W. G., J. C. McWilliams, S. C. Doney. (1994). Oceanic vertical mixing: A review and a model with a nonlocal boundary layer parameterization. *Reviews of Geophysics, 32*(4), 363-403.

LeBel, D. A., W. M. Smethie, M. Rhein, D. Kieke, R. A. Fine, J. L. Bullister, D. Min, W. Roether, R. F. Weiss, C. Andrié, D. Smythe-Wright, E. P.Jones. (2008). The formation rate of North Atlantic Deep Water and Eighteen Degree Water calculated from CFC-11 inventories observed during WOCE. *Deep Sea Research Part I: Oceanographic Research Papers, 55*(8), 891-910.

Liu, J. J. A. Curry. (2010). Accelerated warming of the Southern Ocean and its impacts on the hydrological cycle and sea ice. *Proceedings of the National Academy of Sciences, 107*(34), 14987-14992.

Locarnini, R. A., A. V. Mishonov, J. I. Antonov, T. P. Boyer, H. E. Garcia, O. K. Baranova, M. M. Zweng, D. R. Johnson. (2010). *World Ocean Atlas 2009, Volume 1: Temperature.* (Vol. 1). Washington, D.C.: U.S. Government Printing Office.

Marshall, J., F. Schott. (1999). Open-ocean convection: Observations, theory, and models. *Reviews of Geophysics, 37*(1), 1-64.

Martin, T., W. Park, M. Latif. (2012). Multi-centennial variability controlled by Southern Ocean convection in the Kiel Climate Model. *Climate Dynamics, 40*(7-8), 2005-2022.

Martinson, D. G. (1991). Open ocean convection in the Southern Ocean. In P. C. Chu, J. C. Gascard (Ed.), *Deep convection and deep water formation in the oceans* (pp. 37-52). Amsterdam, The Netherlands: Elsevier Oceanography Series.

Martinson, D. G., P. D. Killworth, A. L. Gordon. (1981). A convective model for the Weddell Polynya. *Journal of Physical Oceanography, 11*(4), 466-488.

Meijers, A. J. S., E. Shuckburgh, N. Bruneau, J.-B. Sallee, T. J. Bracegirdle, Z. Wang. (2013). Representation of the Antarctic Circumpolar Current in the CMIP5 climate models and future changes under warming scenarios. *Journal of Geophysical Research, 117*(12), C12008.

Meincke, J., B. Rudels, H. J. Friedrich. (1997). The Artic Ocean-Nordic Seas thermohaline system. *ICES Journal of Marine Science, 54*(3), 283-299.

Meinshausen, M., S. J. Smith, K. Calvin, J. S. Daniel, M. L. T. Kainuma, J. F. Lamarque, K. Matsumoto, S. A. Montzka, S. C. B. Raper, K. Riahi, A. Thomson, G. J. M. Velders, D. P. P. van Vuuren. (2011). The RCP greenhouse gas concentrations and their extensions from 1765 to 2300. *Climatic Change, 109*(1-2), 213-241.

Milly, P. C. D., A. B. Shmakin. (2002). Global modeling of land water and energy balances. Part I: The land dynamics (LaD) model. *Journal of Hydrometeorology, 3*(3), 283-299.

Ohshima, K. I., Y. Fukamachi, G. D. Williams, S. Nihashi, F. Roquet, Y. Kitade, T. Tamura, D. Hirano, L. Herraiz-Borreguero, I. Field, M. Hindell, S. Aoki, M. Wakatsuchi. (2013). Antarctic Bottom Water production by intense sea-ice formation in the Cape Darnley polynya. *Nature Geoscience, 6*(3), 235-240.

Orsi, A. H., G. C. Johnson, J. L. Bullister. (1999). Circulation, mixing, and production of Antarctic Bottom Water. *Progress in Oceanography, 43*(1), 55-109.

Orsi, A. H., W. M. Smethie, J. L. Bullister. (2002). On the total input of Antarctic waters to the deep ocean: A preliminary estimate from chlorofluorocarbon measurements. *Journal of Geophysical Research, 107*(C8), 3101-3114.

Parkinson, C. L., J. C. Comiso, H. J. Zwally. (1999, updated 2004). Nimbus-5 ESMR Polar Gridded Sea Ice Concentrations. Edited by W. Meier and J. Stroeve. Boulder, Colorado USA: National Snow and Ice Data Center.

Purkey, S. G., G. C. Johnson. (2010). Warming of Global Abyssal and Deep Southern Ocean Waters between the 1990s and 2000s: Contributions to Global Heat and Sea Level Rise Budgets*. *Journal of Climate, 23*(23), 6336-6351.

Purkey, S. G., G. C. Johnson. (2012). Global Contraction of Antarctic Bottom Water between the 1980s and 2000s*. *Journal of Climate, 25*(17), 5830-5844.

Smethie, W. M., A. R. Fine. (2001). Rates of North Atlantic Deep Water formation from chlorofluorocarbon inventories. *Deep Sea Research Part I: Oceanographic Research Papers, 48*(1), 189-215.

Swingedouw, D., T. Fichefet, H. Goosse, M. F. Loutre. (2009). Impact of transient freshwater releases in the Southern Ocean on the AMOC and climate. *Climate Dynamics, 33*(2-3), 365-381.

Taylor, K. E., R. J. Stouffer, G. A. Meehl. (2012). An overview of CMIP5 and the experiment design. *Bulletin of the American Meteorological Society, 93*(4), 485-498.

Visbeck, M. (2009). A Station-Based Southern Annular Mode Index from 1884 to 2005. *Journal of Climate, 22*(4), 940-950.

Whitworth, T., A. H. Orsi. (2006). Antarctic Bottom Water production and export by tides in the Ross Sea. *Geophysical Research Letters, 33*(12), L12609.

Williams, G. D., N. L. Bindoff, S. J. Marsland, S. R. Rintoul. (2008). Formation and export of dense shelf water from the Adélie Depression, East Antarctica. *Journal of Geophysical Research, 113*(4), C04039.

Wüst, G. (1928). Der Ursprung der Atlantischen Tiefenwasser. *Gesellsch. f. Erdkunde, Zeitschrift*, 409-509.

Yin, J. H. (2005). A consistent poleward shift of the storm tracks in simulations of 21st century climate. *Geophysical Research Letters, 32*(18), L18701.

Zenk, W., E. Morozov. (2007). Decadal warming of the coldest Antarctic Bottom Water flow through the Vema Channel. *Geophysical Research Letters, 34*(14), L14607.